Received: 5 May 2022 | Revised: 29 May 2023 | Accepted: 19 June 2023

DOI: 10.1002/qj.4530

Quarterly Journal of the Royal Meteorological Society RMetS

RESEARCH ARTICLE

Assessing the benefit of variational quality control for assimilating Aeolus Mie and Rayleigh wind profiles in NOAA's global forecast system during tropical cyclones

Karina Apodaca[1,2] | **Lidia Cucurull**[2] | **Iliana Genkova**[3] | **R. James Purser**[3] | **Xiujuan Su**[3]

[1]Cooperative Institute for Marine and Atmospheric Studies, University of Miami, Miami, Florida, USA

[2]NOAA/OAR/Atlantic Oceanographic and Meteorological Laboratory, Miami, Florida, USA

[3]I.M. Systems Group, Rockville, Maryland at NOAA/NCEP/Environmental Modeling Center, College Park, Maryland, USA

Correspondence
Karina Apodaca, Spire Global, Inc. Boulder, 1690 38 St, Boulder, Colorado 80301, USA.
Email: karina.apodaca@spire.com

Present address
Karina Apodaca, Spire Global, Inc, Boulder, Colorado USA; and Iliana Genkova, and R. James Purser, Lynker Technologies, LLC, Leesburg, Virginia, USA

Funding information
NOAA/NESDIS/OPPA/Technology Maturation Program under the NOAA-CIMAS, Grant/Award Number: GR003756/665653

Abstract

In this article, we show a "proof-of-concept" study to assess the utility of a variational quality control algorithm in increasing the number of assimilated Aeolus Mie-cloudy and Rayleigh-clear winds in National Oceanic and Atmospheric Administration (NOAA)'s global data assimilation and forecast system. The National Centers for Environmental Prediction (NCEP) Variational Quality Control (NCEP-VQC) algorithm was tuned and applied during the minimization process. This type of quality control uses optimal control theory principles to treat outliers in the probability density function (PDF) of observational departure statistics, assuming that the observation errors follow a family of logistic distributions. In the case of Aeolus Mie-cloudy and Rayleigh-clear winds, the NCEP-VQC algorithm permitted the relaxation of the gross error and one of the recommended ESA quality controls (reject Rayleigh-clear observations below 850 hPa), assigned adaptive observation weights ranging from 0 to 1, and led to an increase in the number of retained Aeolus observations for the calculation of global analyses, which in turn improved the verification statistics on analyzed tropical storms This article discusses the advantage of implementing the NCEP-VQC algorithm in the Aeolus data assimilation, the benefits of retaining more wind profiles that contribute to the analysis calculation, and shows improvements in the initialization and short-term forecasts on several tropical cyclone cases.

KEYWORDS

aeolus, data assimilation, quality control, satellite wind lidar, tropical cyclones, variational

1 | INTRODUCTION

Aeolus, a novel wind mission from the European Space Agency (ESA) launched on August 22, 2018, includes the first space-based Doppler wind lidar (DWL) to date. ALADIN (Atmospheric LAser Doppler INstrument), the main instrument on Aeolus, provides wind profile measurements from a Sun-synchronous, dusk/dawn orbit at

an altitude of 320 km (ESA, 2022). Aeolus aims to provide three-dimensional wind data from the Mie and Rayleigh channels of ALADIN and partially ameliorate the current global observing system data gap (Straume *et al.*, 2020), particularly in the tropics, where tropical cyclones originate. Currently, several operational weather prediction centers assimilate Aeolus Horizontal Line of Sight (HLOS) wind profiles and have reported various degrees of model forecast skill improvement (e.g., at the European Centre for Medium-Range Weather Forecasts [ECMWF] – Rennie *et al.*, 2021). Furthermore, at the National Centre for Medium-Range Weather Forecasts, Aeolus wind observations have reduced cyclone position errors, as George *et al.* (2021) described in one cyclone case study in the Arabian Sea. Even though Aeolus observations are not assimilated operationally at the National Oceanic and Atmospheric Administration (NOAA), several studies have demonstrated the value of this dataset in improving global weather forecast skill using earlier versions of the National Centers for Environmental Prediction/Global Forecast System with the Cubed Sphere dynamical core (NCEP/GFS-FV3, Liu *et al.*, 2022, Apodaca *et al.*, 2020). Furthermore, benefits from the assimilation of Aeolus observations have also been found in hurricane prediction at NOAA using the regional Hurricane Weather Forecasting system (HWRF, Marinescu *et al.*, 2022).

Developing optimal quality control strategies is key to maximizing the benefits of assimilating a new observation type, such as Aeolus HLOS, especially when these data can improve the initialization of tropical cyclones (TCs) and other severe weather events. Inaccurate a-priori estimates of the state of the atmosphere under complex flow structures combined with the use of suboptimal quality control (QC) procedures can have detrimental impacts on the analysis. The sole use of static QC and background quality control, which are based on blacklisting and background-based rejections, can result in poor choices (i.e., keeping observations with initially large background departures, rejecting correct observations because departures from the background are large and/or assigning incorrect weights to some observations).

With the goal of better assimilating Aeolus's observations, in this article, we show a "proof-of-concept" study to assess the utility of a Variational Quality Control (VarQC) algorithm (Purser, 2018). This VarQC algorithm is already included in the global data assimilation system component of the GFS_v16 (NCEP-VQC, hereafter), implemented operationally at NOAA in March 2021 (Farrar, 2021), and it is routinely applied to conventional/surface observations. We saw that the characteristics of the NCEP-VQC algorithm, described next, could improve the quality control of Aeolus observations. In particular, the Rayleigh-clear and Mie-cloudy channels are of superior quality to Rayleigh-cloudy and Mie-clear channels observations (Martin *et al.*, 2021; Zuo *et al.*, 2022). The measurements from the Rayleigh channel have better performance in a clear sky (Rayleigh-clear), for which there is little or no contamination from Mie scattering; the wind measurements in the Mie channel need strong backscattering from aerosols, water droplets, or ice crystals (Mie-cloudy) (Rennie *et al.*, 2020). Rayleigh-clear and Mie-cloudy winds are currently the only two types of Aeolus winds that are assimilated into the ECMWF model for operational weather forecasts (Rennie *et al.*, 2021). Furthermore, at the accumulation length of Aeolus (~90 km), the less-accurate Rayleigh-clear channel provides up to four times more observations than the Mie-cloudy channel (Savli *et al.*, 2019). Based on these considerations, only Rayleigh-clear and Mie-cloudy winds were extracted to evaluate and apply VarQC in our study.

The NCEP-VQC algorithm is analogous to the Huber norm quality control used in the ECMWF/4D-Var system (Tavolato and Isaksen, 2014). However, the NCEP-VQC algorithm uses a family of smooth generalized logistic distributions to describe the statistics of the observation errors of conventional observations. For each member of the generalized logistic family, there is an analogous (practically equivalent) Huber distribution. The distinguishing characteristic of the Huber model is that, for a finite range of moderate values of the observational error, the probability is assumed to remain exactly Gaussian, with modeling of the tails outside of this range done using some other analytic function suitable for fatter tails. For the logistic family, the transition to fatter tails is smooth and continuous, so the Gaussian behavior only occurs in the limit when the observation error is close to zero. For observation departures with probability density functions (PDF) that resemble (and generalize) logistic distributions, the NCEP-VQC algorithm computes three parameters: broadness, asymmetry, and convexity that quantify the attributes of the tails of the density function once its mode has been recentered and its spread standardized by rescaling. These parameters are related to the higher moments of the standardized distribution that control the skewness and kurtosis of the observation error (OE). These calculations are performed during the minimization process using optimal control theory principles to treat the outliers that might exist in the PDF of departure statistics. The VarQC algorithm allows for the relaxation of gross error quality controls by assigning observation weights on a range from 0 to 1. A weight closer to 0 means observations have the least impact on the calculation of an analysis. Conversely, a weight closer to 1 indicates observations have a stronger influence on an analysis. The Bayesian principles that underlie the VarQC techniques can be found in

Lorenc and Hammon (1988), Ingleby and Lorenc (1993), and Andersson and Järvinen (1999).

This article is organized as follows: in Section 2, we provide Aeolus data specifications and a discussion on the OE as provided by departure statistics. The global model configuration and experimental design are presented in Section 3, and the results are discussed in Section 4. Lastly, conclusions are provided in Section 5.

2 | AEOLUS OBSERVATIONS AND INNOVATION STATISTICS

For the experiments described in Section 4, we assimilated only vertical profiles of HLOS winds in the Rayleigh-clear and Mie-cloudy channels. We used the Level-2B, version 10 product, with the "M1" telescope primary mirror wind bias correction (Weiler *et al.*, 2021). We applied the static quality controls described in Rennie and Isaksen (2020) and did not include any additional bias correction. However, instead of always applying the QC flag that rejects Rayleigh-clear observations at pressures larger than 850 hPa, VarQC was introduced to dynamically retain some observations with larger observation departures, as compared to the limit acceptable by the background quality control, at these high-pressure levels. We employed the depth of bin or signal-to-noise ratio QC to eliminate poor quality observations regardless of the potential of impacting the shape PDF of observation departures of Aeolus data. The main reason behind these choices was to test the benefit of the NCEP-VQC algorithm in the lower troposphere where TCs form and to maximize the number of available observations before the assimilation process.

ECMWF observation error inflation was applied to both Mie-cloudy and Rayleigh-clear channels, as Rennie and Isaksen (2020) described. Carefully examining the innovation statistics at the analysis times provides valuable information needed to select a suitable error model (Tavolato and Isaksen, 2014). For this purpose, samples of observations minus background (O-B) innovations were obtained from a total of 120 six-hourly forecasts with Mie-cloudy and Rayleigh-clear observations used in monitoring mode (i.e., without these observations being assimilated). These innovation statistics were estimated for the period of August–September 2019. This time period was chosen because other NWP centers used the same Aeolus observations, and we wanted to facilitate comparisons with results from other studies. During these two months, there were periods without significant tropical cyclone activity. Therefore, innovation statistics for periods of low TC activity, a total of 120 six-hourly forecasts, were used as a benchmark for obtaining a probability model for the observation errors and for obtaining sets of PDF moments needed to tune the modulating parameters (asymmetry, broadness, and convexity) of the NCEP-VQC algorithm. An assessment of (O-B) PDFs for Mie-cloudy and Rayleigh-clear wind observations pointed to unimodal and leptokurtic distributions with minor skewness (asymmetry). The characteristics of this type of error model are suitable for the logistic Are the family of distributions in the NCEP-VQC algorithm. After several tuning experiments, we found a set of distribution moments that provided reasonable weight distributions as a function of observation departures. For the final NCEP-VQC configuration, we selected values of variance and kurtosis of 19 and 4 for Mie-cloudy winds and 27 and 5 for Rayleigh-clear winds. Asymmetry was set to 0; the initial gross error was set to $4\,m{\cdot}s^{-1}$, and the minimum/maximum OE range was set to $2–10\,m{\cdot}s^{-1}$. The NCEP-VQC algorithm uses initial values of variance and kurtosis. After performing eight sensitivity (tuning) experiments, we varied the broadness and kurtosis values. To do so, we calculated the standard deviation of all the moments of the PDF of innovation statistics and the standard deviation of the OE limits. The VarQC had not been significantly tested on satellite winds before. Therefore, a conservative approach was appropriate. We chose values for variance and kurtosis – along with minimum and maximum errors – within approximately 0.5 to 1.0 sigma. We selected these values as they allowed more observations to pass the background quality control compared to the other tuning experiments and to an experiment without VarQC, which was treated as a baseline. They showed improved cost function reduction without increasing the spread of (O-A) innovation statistics. If NOAA eventually decides to assimilate Aeolus operationally and apply VarQC to their assimilation, we recommend tuning experiments whereby the error limits for the background quality control check are increased to larger sigma values. In Figure 1a,b, we show an example of PDF histograms of innovation values for the Mie-cloudy and Rayleigh-clear HLOS wind observations valid on August 20, 2019 at 1800 UTC. The red curve is the Gaussian best fit. Even though the Aeolus data had already undergone strict static quality controls and the "M1" bias-corrected dataset was used, data outliers for the Mie-cloudy and Rayleigh-clear channels remained. Similar behavior was found during other cycles.

3 | GLOBAL MODEL CONFIGURATION AND EXPERIMENTS

This study used the GFS_v16.0 version of NCEP's global data assimilation and forecast system. The data assimilation framework is a hybrid 4DEnVar system

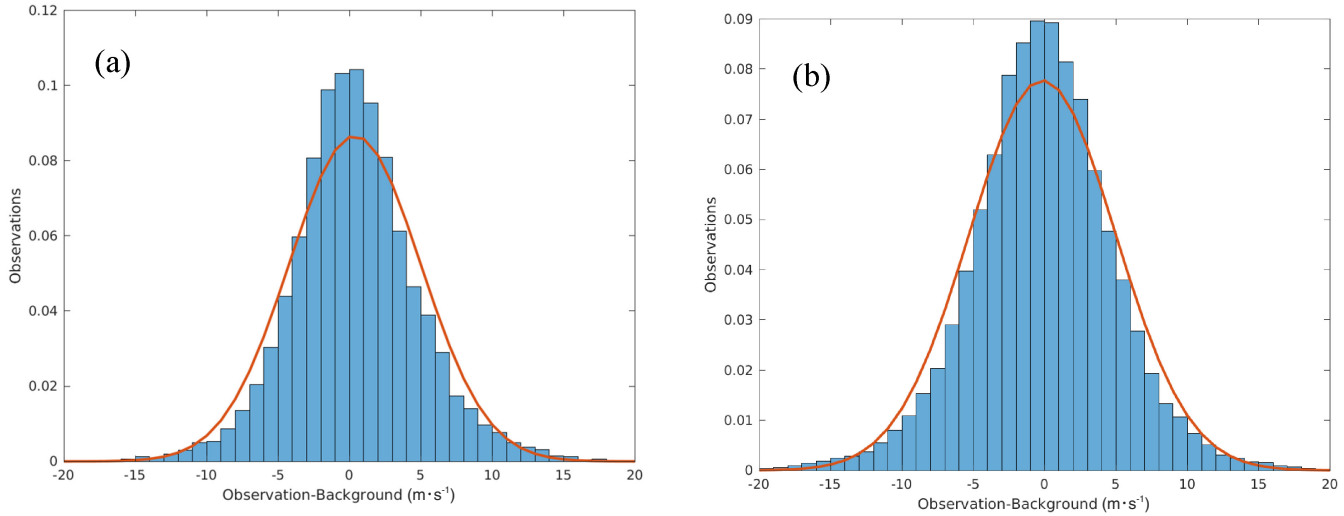

FIGURE 1 Aeolus innovation statistics, for (a) Mie-cloudy (b) Rayleigh-clear used, valid at, Mie-cloudy all, valid on August 20, 2019 at 1800 UTC, from 250 to 850 hPa, globally. The best Gaussian fit distribution is shown in red. Aeolus data include the "M1" principal mirror temperature bias correction [Colour figure can be viewed at wileyonlinelibrary.com]

TABLE 1 GFS_v16.0 configuration.

Model	NOAA/NCEP FV3GFS_v16.0
DA framework and specifications	Hybrid 4DEnVar, 80 member ensemble
Model resolution	Deterministic: C384, EnKF: C192, vertical: L127
Analysis and forecast resolution	.25° or approximately 25 km, horizontal, up to 80 km, vertical
New data for assessment	Aeolus HLOS winds, L2B product, M1 BC, Mie (cloudy), Rayleigh (clear)

TABLE 2 Configuration settings for the observing system experiments

Experiments	Period/dates	Data, OBS error, QC, BC
AEOLUS	**FM-B period:** September 17–24, 2019	NCEP operational data assimilation suite AEOLUS L2-B ECMWF OE inflation tuned for GFS ESA static QC No additional BC
AEOLUS+VarQC	**FM-B period:** September 17–24, 2019	NCEP operational data assimilation suite AEOLUS L2-B ECMWF OE inflation tuned for GFS ESA static QC VarQC No additional BC

(Kleist and Ide, 2015), which was upgraded to use a local ensemble Kalman filter for the ensemble component, with a total of 80 ensemble members. This system includes the Gridpoint Statistical Interpolation system (Derber *et al.*, 1991) to assimilate observations, including Aeolus winds, with the NCEP-VQC algorithm.

We employed a forecast/background resolution of C384 (~25 km grid size) in the deterministic component. The analysis increment is computed in the linear Gaussian grid consistent with C192 (~50 km grid size) in the ensemble component. Lastly, the model employed 127 levels in the vertical, with a model top of up to 80 km. It is important to note that due to constraints in computing resources, the resolution used in this study was coarser than the one used in NCEP/Operations, but the benefits of assimilating a new observation type – and applying VarQC, as in this case – can still be assessed. The global model configuration settings are summarized in Table 1.

We conducted two experiments to evaluate the impact of assimilating Aeolus observations with the additional VarQC. The first experiment, named AEOLUS, included the suite of operational observations assimilated by NOAA/NCEP at the time of the study, along with the assimilation of Mie-cloudy and Rayleigh-clear wind profiles with the ESA-recommended QCs (Weiler *et al.*, 2021). The second experiment, AEOLUS + VarQC,

TABLE 3 2019 tropical cyclone cases

Storm name	Basin	Dates	Storm category at peak intensity
Dorian	AL	August 24–September10	Category 5 hurricane
Erin	AL	August 26–29	Tropical storm
Humberto	AL	September 13–19	Category 3 hurricane
Imelda	AL	September 17–19	Tropical storm
Jerry	AL	September 17–23	Category 2 hurricane
Kiko	EP	September 12–24	Category 4 hurricane
Lorena	EP	September 17–22	Category 1 hurricane
Mario	EP	September 17–22	Tropical storm

Abbreviations: AL, Atlantic; EP, East Pacific.

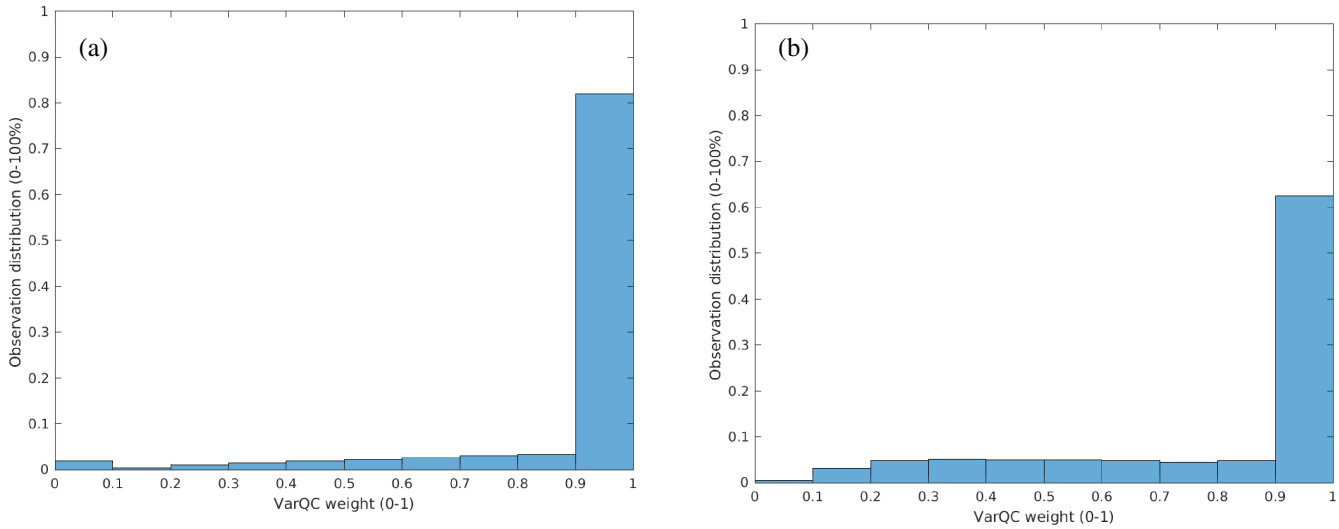

FIGURE 2 VarQC adaptive weight distribution of Aeolus observations for (a) Mie, cloudy, and (b) Rayleigh, clear winds, valid on August 20, 2019 at 1800 UTC [Colour figure can be viewed at wileyonlinelibrary.com]

had the same configuration as AEOLUS but assimilated Mie-cloudy and Rayleigh-clear data with the additional VarQC. Other settings for these experiments are detailed in Table 2. These experiments were conducted from September 17 to 24, 2019, coinciding with several tropical cyclone cases (Table 3).

4 | RESULTS

4.1 | Adaptive weights

As noted in Sections 1 and 2, an observation weight closer to 1 means the most observational impact on the analysis, and conversely, a weight closer to 0 indicates the least impact. For illustrative purposes, we show in Figure 2 how the NCEP-VQC algorithm assigns observation weights in an adaptive manner. The observation weight distribution of the Mie-cloudy and Rayleigh-clear data were plotted for each analysis cycle of the experiments described in Table 3. In Figure 2a,b, for August 20, 2019 at 1800 UTC assimilation cycle, approximately 20% of the Mie, cloudy and about 40% of Rayleigh, clear observations with larger departures are assimilated globally, but with a reduced VarQC weight as compared to observations with smaller departures. Similar weight distributions were observed during approximately 90% of the assimilation cycles. We also plotted the values of the observation innovation (O-B) in $m \cdot s^{-1}$ against the VarQC weight as indicated in Figure 3a,b; we further confirmed that for smaller innovation values located at the peaks of the distributions, the NCEP-VQC algorithm assigned a weight close to one, but for larger (O-B) values, the observation weights were reduced for both Mie-cloudy and Rayleigh-clear channels. Figures 2 and 3 clearly indicate that outliers were allowed to influence the analyses but with a reduced observation weight.

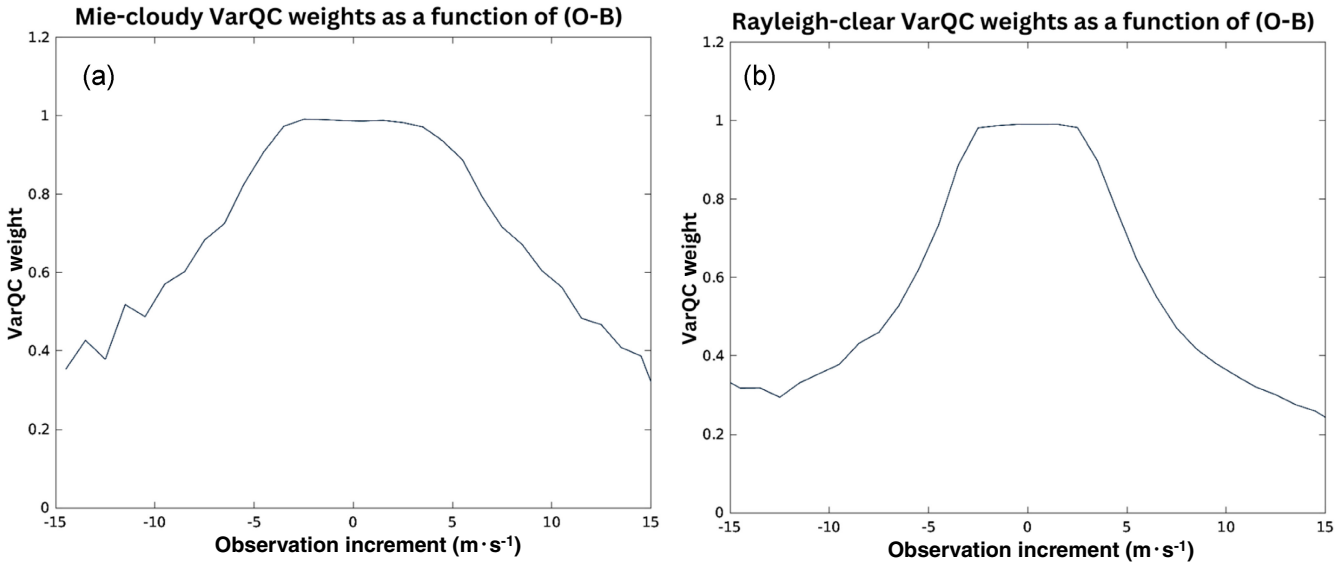

FIGURE 3 Values of VarQC weight as a function of observation innovation (O-B) in $m \cdot s^{-1}$ for (a) Mie-cloudy and (b) Rayleigh-clear winds, valid on August 20, 2019 at 1800 UTC [Colour figure can be viewed at wileyonlinelibrary.com]

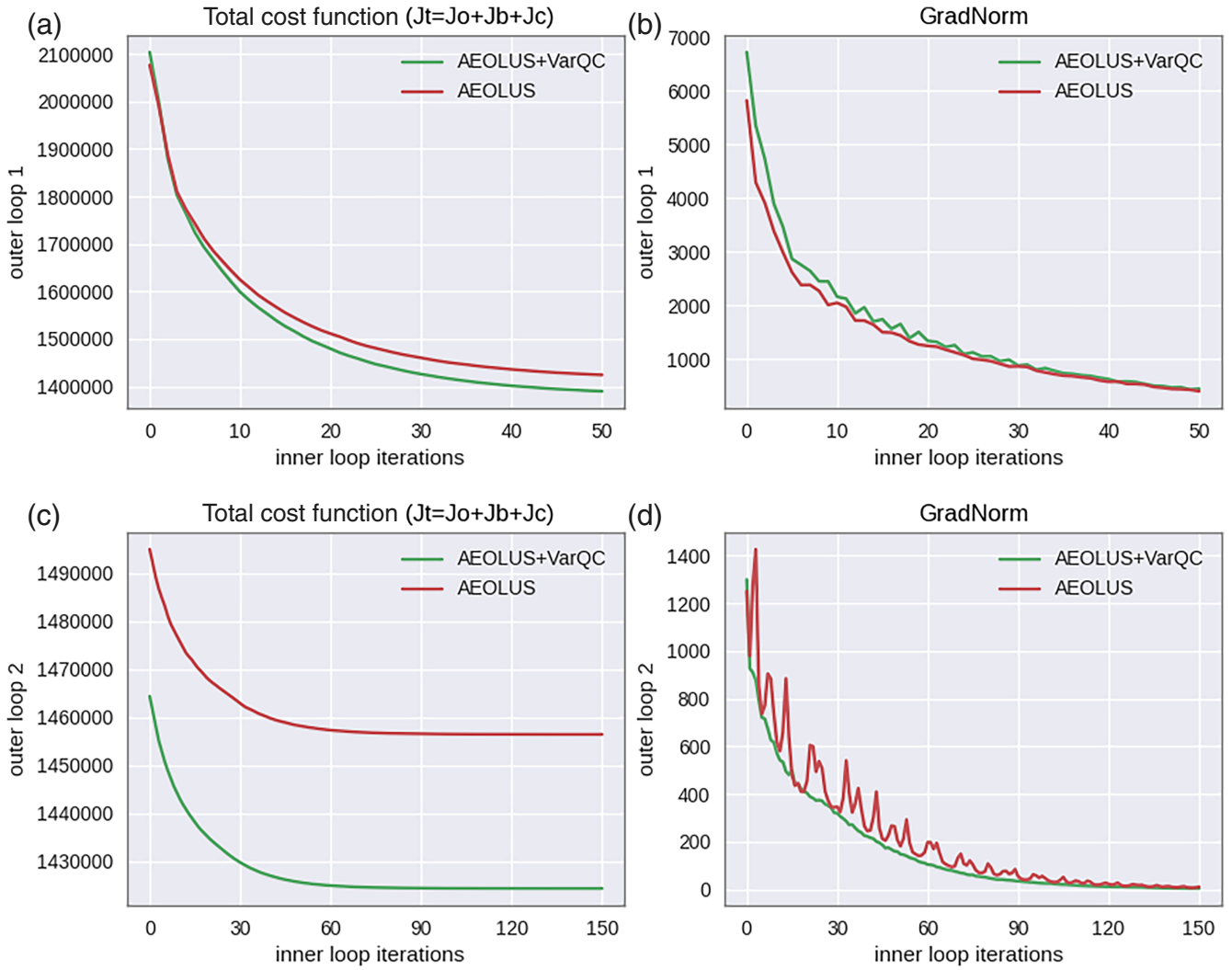

FIGURE 4 Cost function (a) and (b) and gradient norm curves (c) and (d) for the AEOLUS (red) and AEOLUS + VarQC (green) experiment [Colour figure can be viewed at wileyonlinelibrary.com]

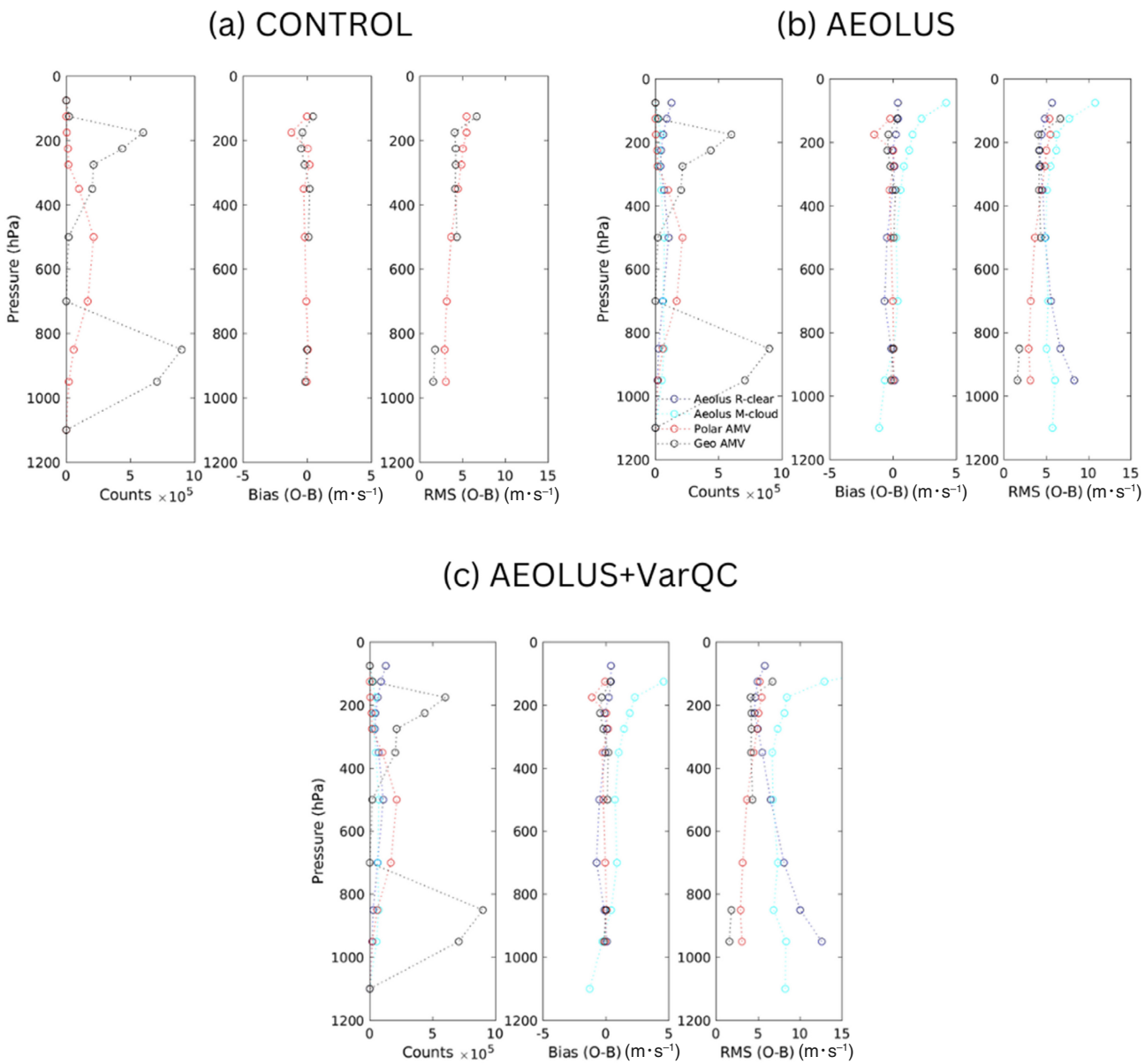

FIGURE 5 One-week averaged vertical profiles of the number of observations, (O-B), (O-A) bias and root-mean-square error for Aeolus and other wind observations: (a) CONTROL; (b) AEOLUS; (c) AEOLUS + VarQC [Colour figure can be viewed at wileyonlinelibrary.com]

4.2 | Cost function and gradient norm statistics

Cost function and gradient norm statistics generally show the overall performance of the minimization procedure and can indicate if there are conditioning issues. We plotted the cost function and its gradient norm, as a function of the number of iterations, set to 150 for the first and second outer loops for 38 analysis cycles of the AEOLUS and AEOLUS + VarQC experiments. Decreasing curves and convergence as a function of iteration number are positive indicators of the benefit of assimilating Aeolus data. For example, Figure 4a,c shows a comparison valid on September 17, 2019 at the 0000 UTC cycle. During this cycle, the assimilation of Aeolus data with VarQC further reduced the final cost function from about 1,460,000 to 1,430,000. These plots also reveal that the system settings of the AEOLUS + VarQC experiment resulted in the best performance. Figure 4b indicates that the calculation of the gradient produces a "zig-zag" pattern on the curve for only the AEOLUS experiment, which is not present in Figure 4d. The treatment of large innovation values could cause this behavior, resulting in large gradient norm spikes. However, any causes, like occasional minimization problems in the operational GFS (Daryl T. Kleist – NOAA/Environmental Modeling Center, personal communication), could require further investigation. Nonetheless, the AEOLUS + VarQC experiment

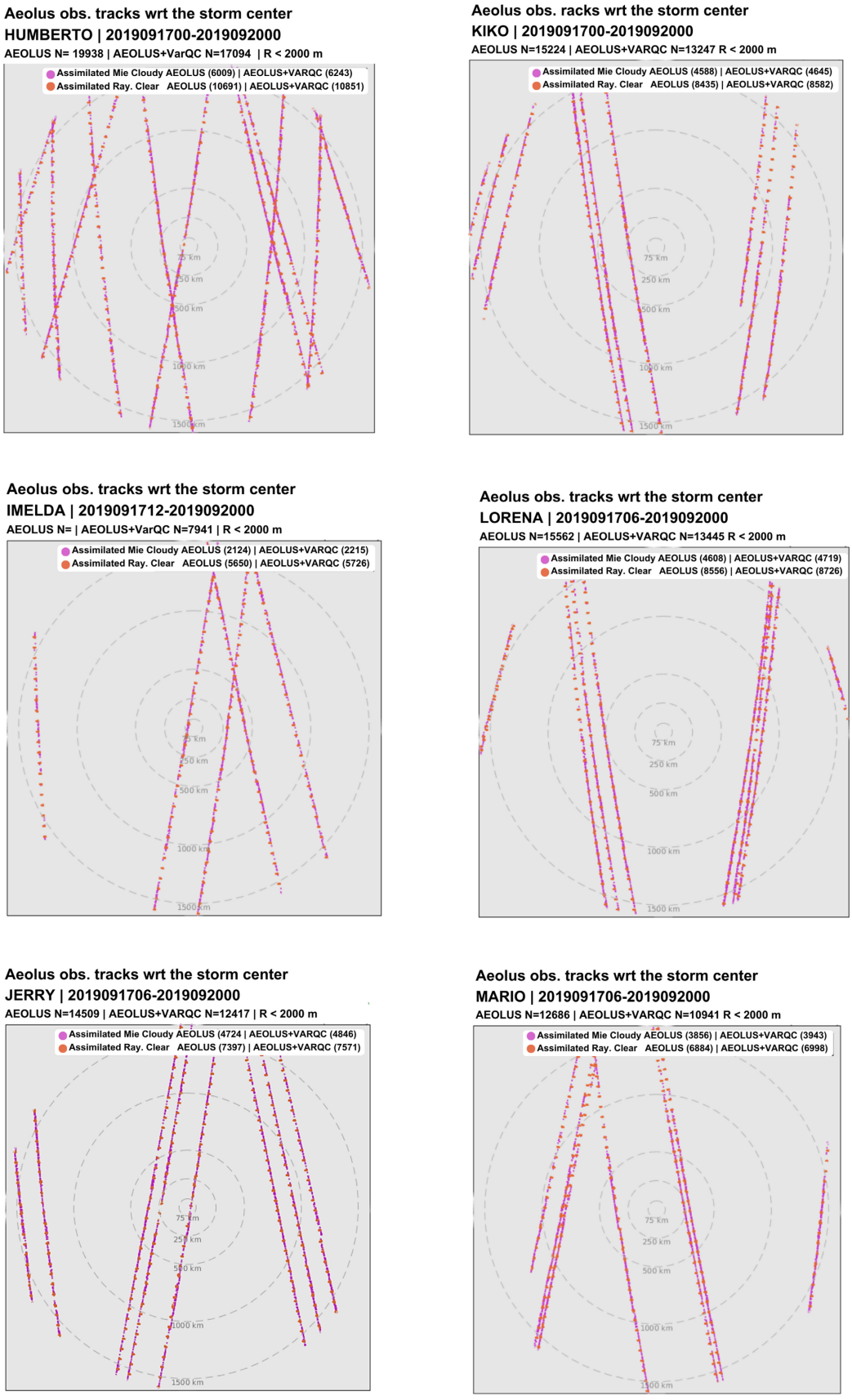

FIGURE 6 Swaths of assimilated observations with respect to the storm center during the life cycle of six tropical cyclones. *N* equals globally assimilated observations. Numbers in parentheses indicate assimilated Mie-cloudy and Rayleigh-clear observations for the AEOLUS and AEOLUS + VarQC experiments [Colour figure can be viewed at wileyonlinelibrary.com]

shows better performance. Similar behavior was observed during approximately 90% of the assimilation cycles.

4.3 | Vertical distribution of departures for assimilated Aeolus observations

The distribution of observation departures as a function of height in pressure coordinates was investigated during each analysis cycle for the AEOLUS and AEOLUS + VarQC experiments. This process showed vertical layers where the VarQC could impact the assimilation of Aeolus observations the most. An evaluation during 28 cycles indicated that, on average, observation increments tend to be larger near the 250 hPa and 850 hPa model vertical levels, followed by impacts near the 400 hPa level. The vertical distribution of assimilated Aeolus observations also resulted in higher numbers of assimilated

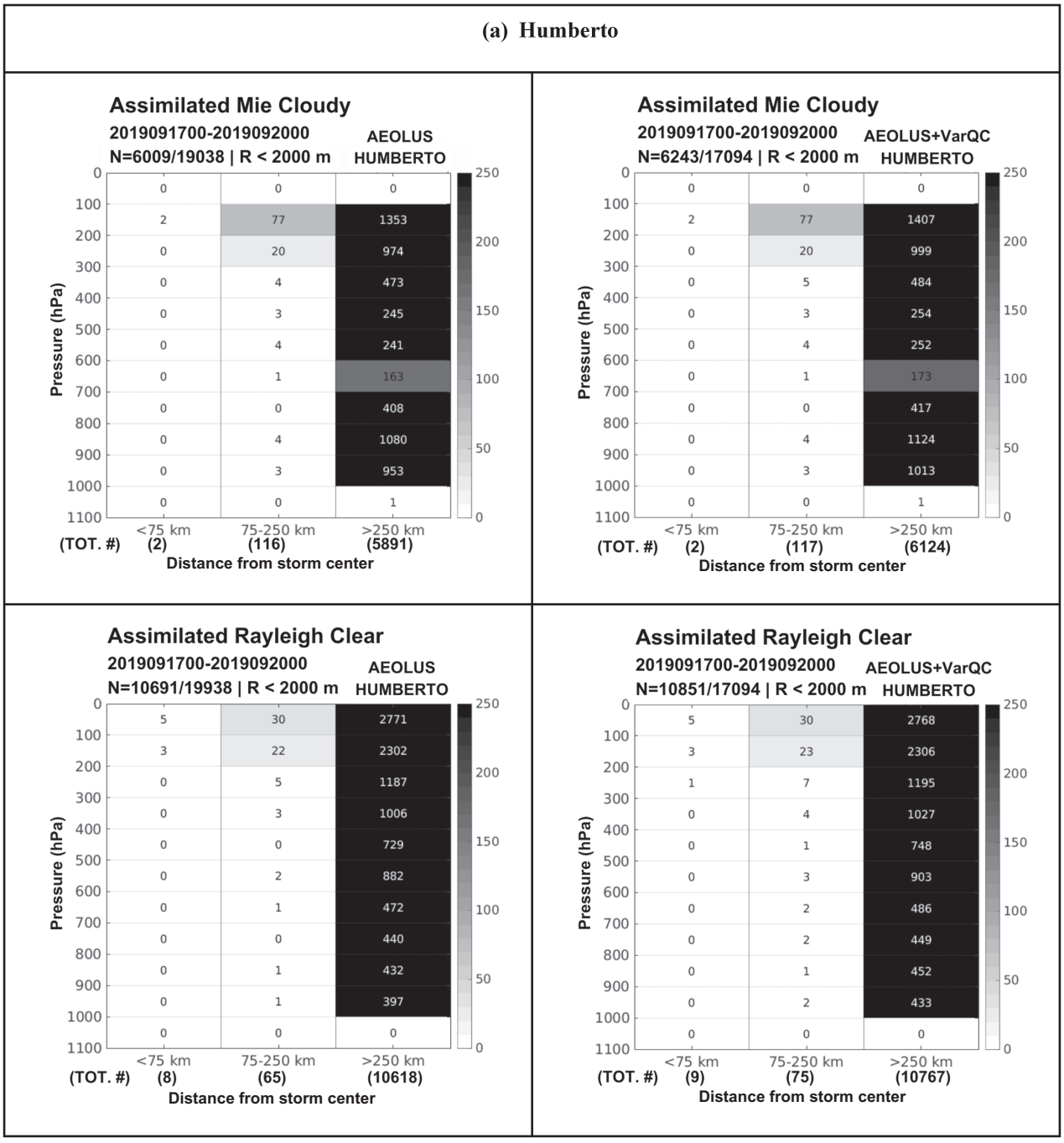

FIGURE 7 Assimilated Mie-cloudy and Rayleigh-clear observations as a function of height in hPa and distance from the storm center in km, for 2019: AL basin TCs *Humberto*, *Imelda*, and *Jerry*, for the AEOLUS (left) and AEOLUS + VarQC (right) experiments. *N* equals the ratio of near-storm assimilated to globally assimilated observations

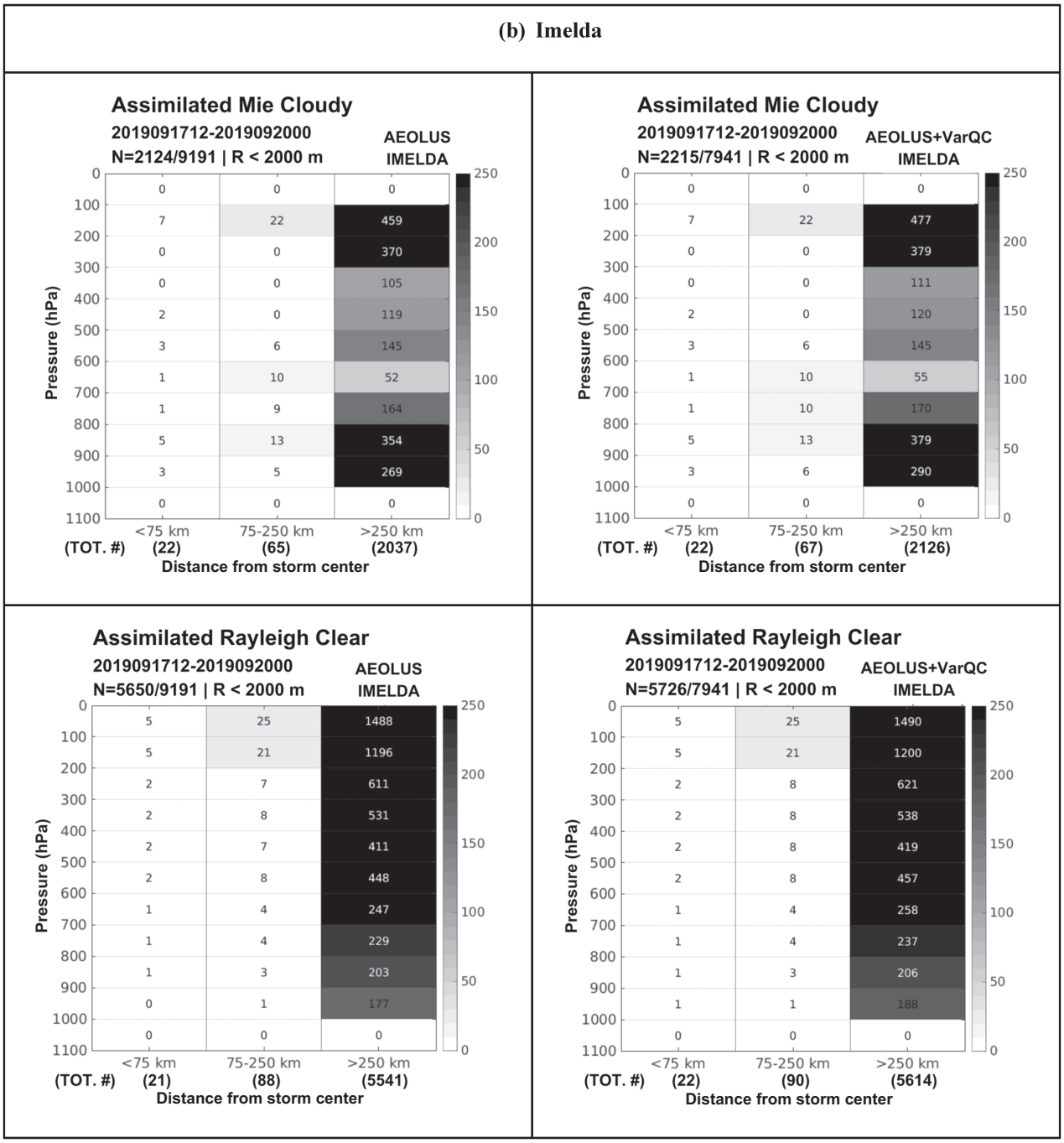

FIGURE 7 (Continued)

observations at these levels. Analysis residuals (O-A) indicated smaller departure values after data assimilation but with minor magnitudes and nearly indistinguishable from (O-B). In Figure 5a–c, we show one-week averaged profiles of the number of assimilated observations, and (O-B) bias, and root-mean-squared (RMS) errors. The former metrics are for satellite wind-measuring observing systems, such as geostationary and polar atmospheric motion vectors (AMVs) from a set of AEOLUS, and AEOLUS + VarQC experiments, with an additional CONTROL experiment. Please note that Aeolus wind data were present only in the former two experiments. Still, all three of them had otherwise identical configurations and included the NCEP operational suite of observations.

Figure 5a shows the profiles of the wind-observing systems assimilated in the CONTROL experiment (without Aeolus); the similarities seen in the profiles with respect to Figure 5b,c indicate that the assimilation of Aeolus did not affect the assimilation of other wind

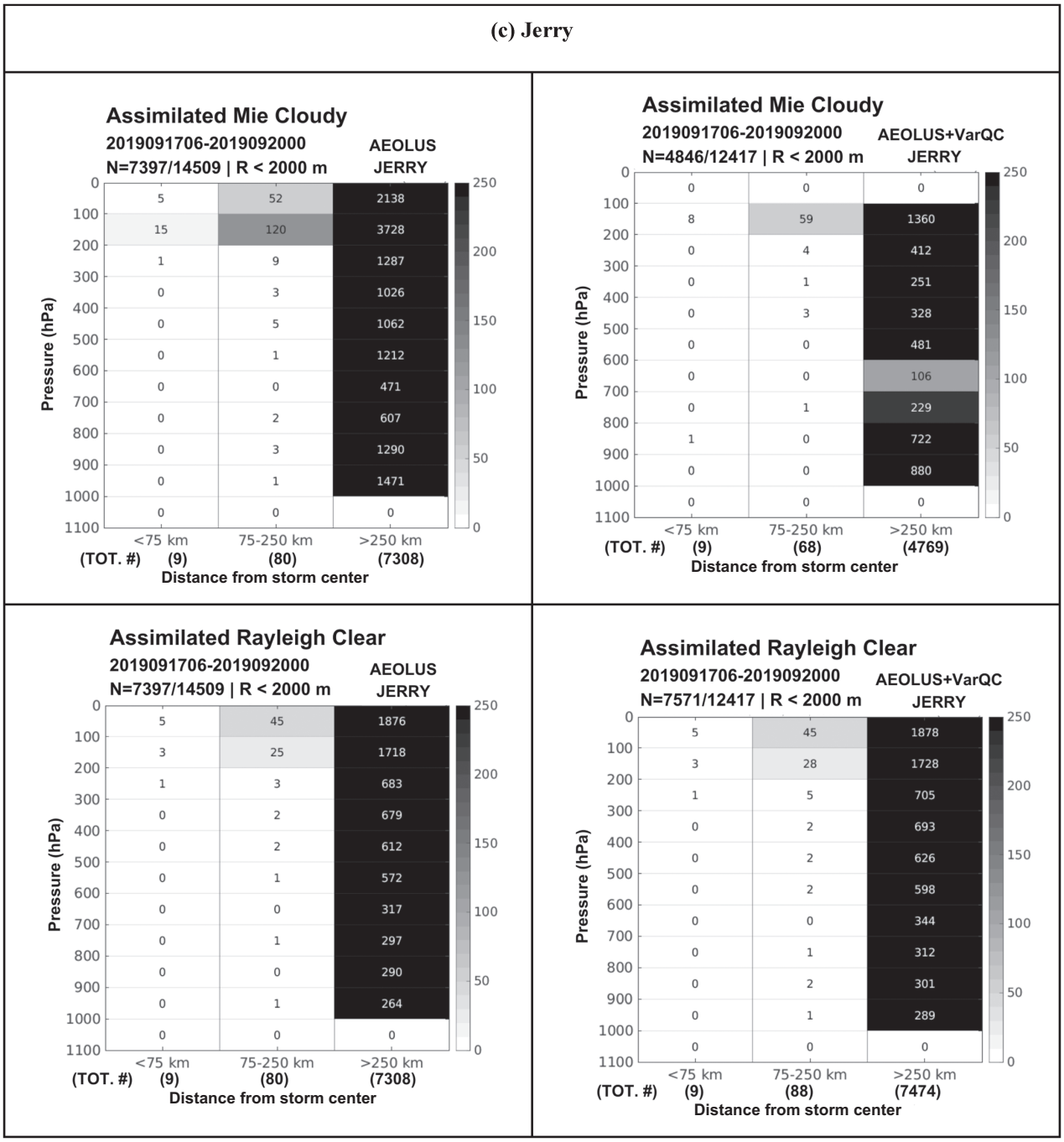

FIGURE 7 (Continued)

observations. Figure 5b,c show the profiles of the Aeolus (O-B) bias (middle) and RMS error (right). The observation increment of Aeolus profiles was comparable to that in the other wind-observing systems, in both the AEOLUS and AEOLUS+VarQC experiments. A reversal in the profile magnitudes for Mie-cloudy and Rayleigh-clear is in agreement with other studies (e.g., Marinescu *et al.*, 2022), indicating that Mie-cloudy winds were more biased in the upper atmosphere where the retrieval algorithm has errors due to processing of faster winds and the Rayleigh-clear winds were more biased in the lower atmospheric levels due to the interaction with clouds and surface. The week-long average also revealed larger RMS error values in AEOLUS + VarQC compared to the AEOLUS experiment. This behavior is expected because the VarQC mechanism allowed the assimilation of observation outliers in the analysis calculation but with reduced weight. Also, note we included Mie-cloudy winds at levels above 850 hPa in Figure 5c. In Section 4.4, we show that despite the

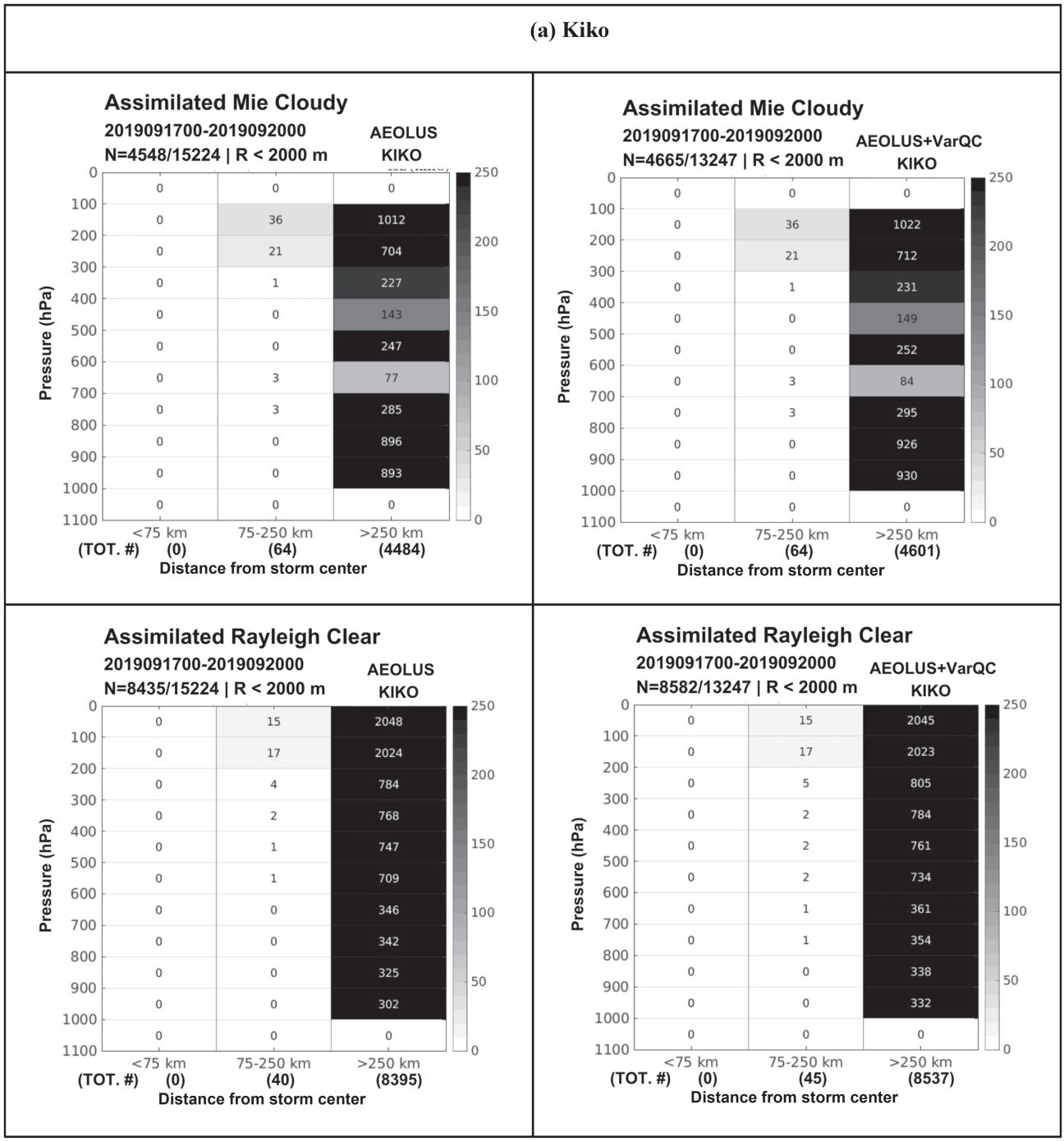

FIGURE 8 Assimilated Mie-cloudy and Rayleigh-clear observations as a function of height in hPa and distance from the storm center in km, for 2019: EP basin TCs (a) *Kiko*; (b) *Lorena*; (c) *Mario*

increased RMS errors, the AEOLUS + VarQC assimilation approach benefited the forecasts of TC. It is likely that permitting the assimilation of possibly flawed observations, or those that deviate significantly from the model background, does not necessarily reflect the quality of the foreca st (Brett Hoover – NOAA/Environmental Modeling Center, personal communication). In regions where observations are sparsely located, it is better to assimilate "down-weighted" observations.

4.4 | Impact on the number of assimilated observations and short-range forecasts during tropical cyclones

A total of six TC cases, three in the Atlantic (AL) and three in the East Pacific (EP) basins, were evaluated. Details on these storms are provided in Table 3. These storms were selected because they exhibited various categories at peak intensity, ranging from tropical storms to hurricanes 2–4

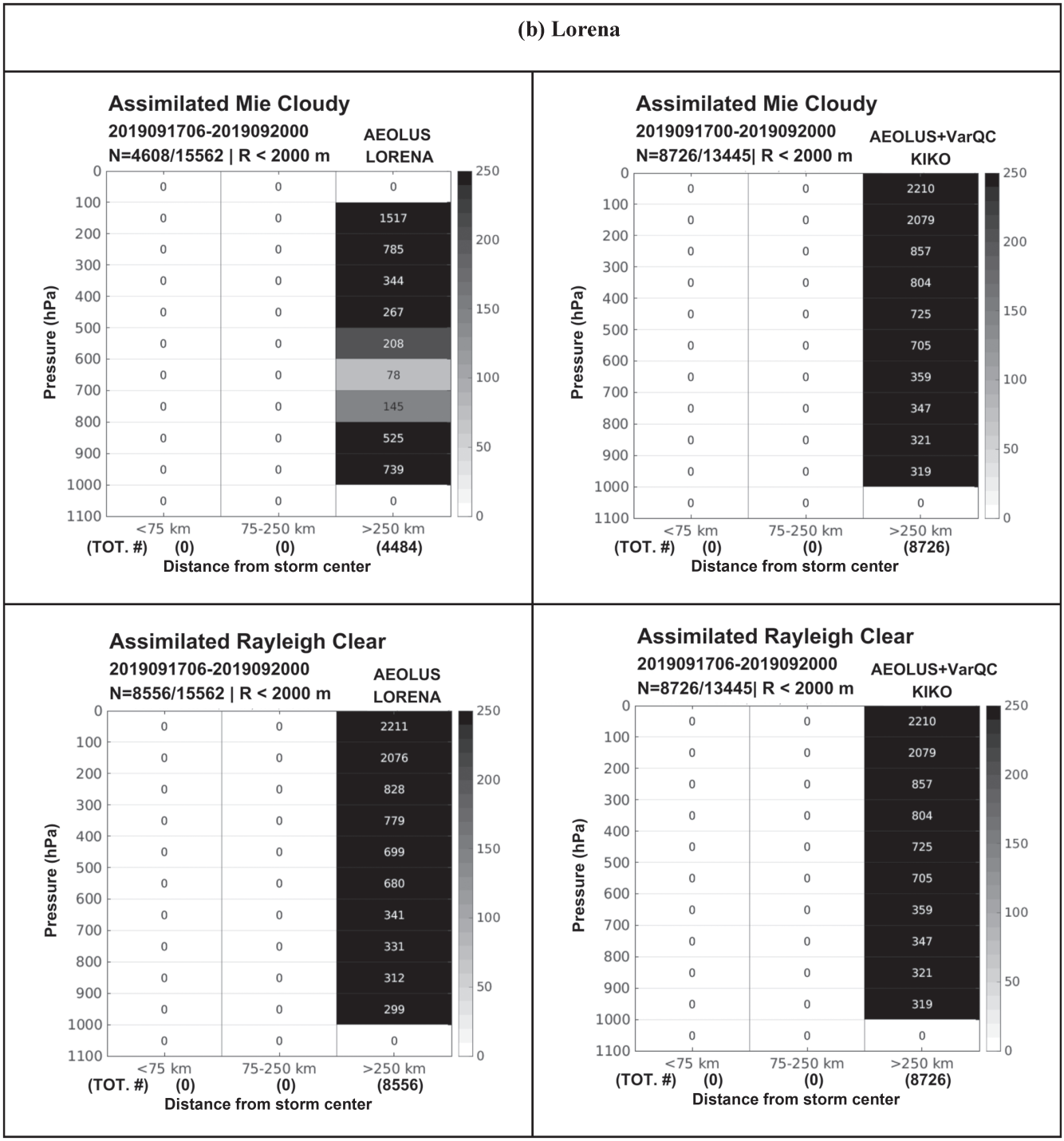

FIGURE 8 (Continued)

on the Saffir–Simpson scale. Some cyclones were highly sampled by reconnaissance aircraft, while others were not, particularly in the EP basin. Consequently, the assimilation of Aeolus wind profiles was expected to bring additional information content in generating the analysis. Verification was done with the global model version of the GROOT-G package (OSEs and OSSEs on TCs, n.d) package. This verification software creates a storm-centered pseudo-nest with a radius of 2000 km. GROOT-G can check whether observations are present within 2000 km of the storm center and generate storm-relative graphics that allow a near-storm environment assessment of the impact of observations. In Figure 6, we can see storm-relative plots with swaths of the assimilated Mie-cloudy and Rayleigh-clear wind profiles that passed the background QC, for the 2019 AL storms *Humberto*, *Imelda*, and *Jerry*, and EP basin storms *Kiko*, *Lorena*, and *Mario*, during the lifetime of these storms. Since the location of the Aeolus

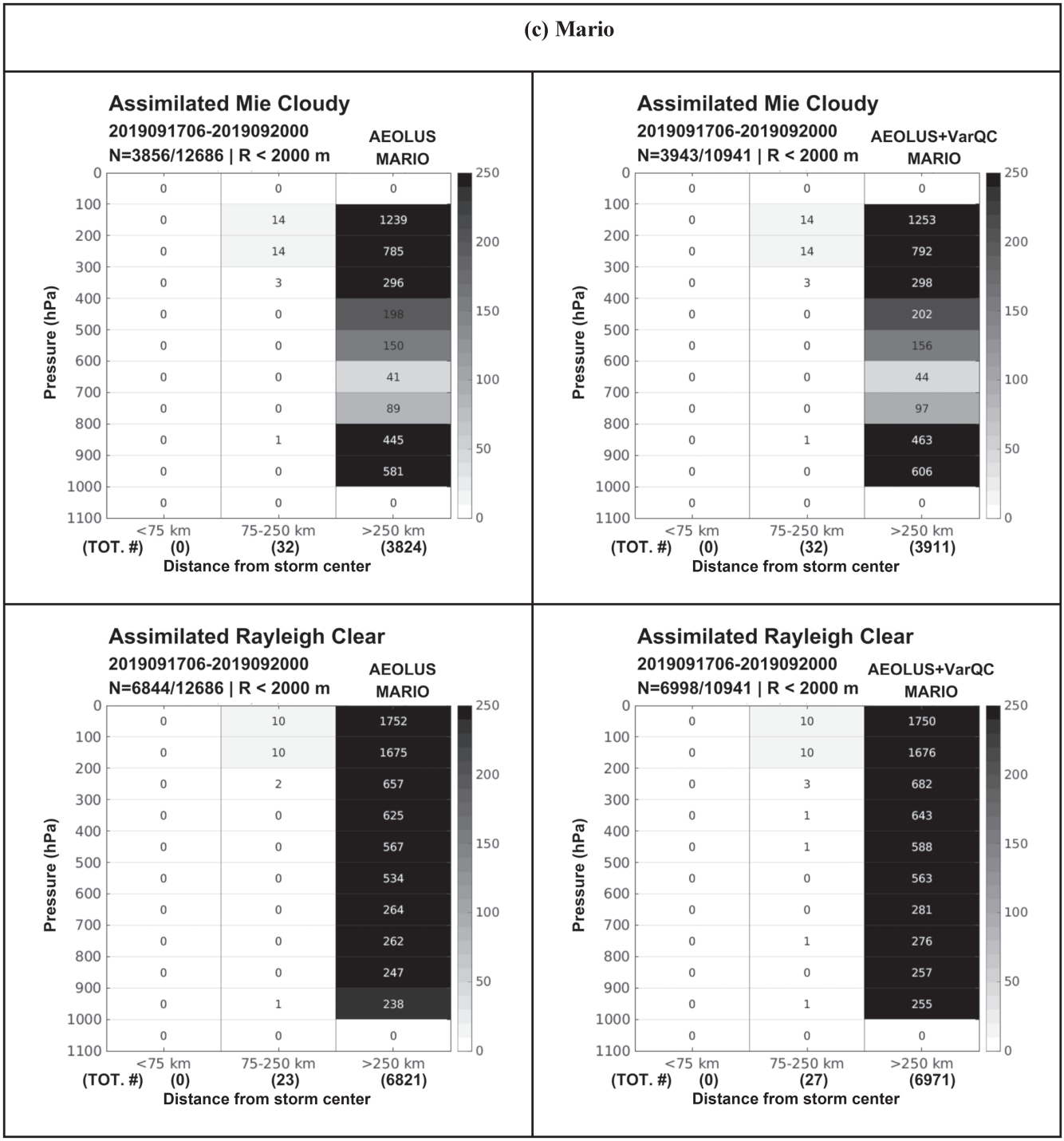

FIGURE 8 (Continued)

swaths is identical for both the AEOLUS and the AEOLUS + VarQC experiments, we also show in Figures 7 and 8 the number of assimilated profiles as a function of height in hPa and distance from the storm center in km for the six storms. A comparison of the number of assimilated HLOS wind profiles on these cases indicated that applying VarQC led to an overall increase in the number of assimilated Mie-cloudy and Rayleigh-clear wind profiles. Approximately 100–200 additional profiles relative to each TC center were assimilated in the AEOLUS + VarQC experiment during the lifetime of each storm. The number of assimilated Mie-cloudy and Rayleigh-clear profiles for all TC cases is shown in Table 4. Moreover, Figures 7 and 8 revealed a high storm-to-storm variability on the location of the assimilated Mie-cloudy and Rayleigh-clear profiles relative to the storm center. Further investigation

TABLE 4 Number of assimilated (passed first guess check) Mie-cloudy and Rayleigh-clear observations for 2019 Atlantic (AL) and East Pacific (EP) storms for the AEOLUS and AEOLUS + VarQC experiments. Note the increased number of assimilated wind profiles in all TC cases when applying VarQC

	Mie-cloudy		Rayleigh-clear	
Name	**AEOLUS**	**AEOLUS + VarQC**	**AEOLUS**	**AEOLUS + VarQC**
2019 Atlantic Basin TCs				
Humberto	6,009	6,243	10,691	10,851
Imelda	2,124	2,215	5,650	5,726
Jerry	4,724	4,846	7,397	7,571
2019 East Pacific Basin TCs				
Kiko	4,548	4,665	8,435	8,582
Lorena	4,608	4,719	8,556	8,726
Mario	3,856	3,943	6,844	6,998

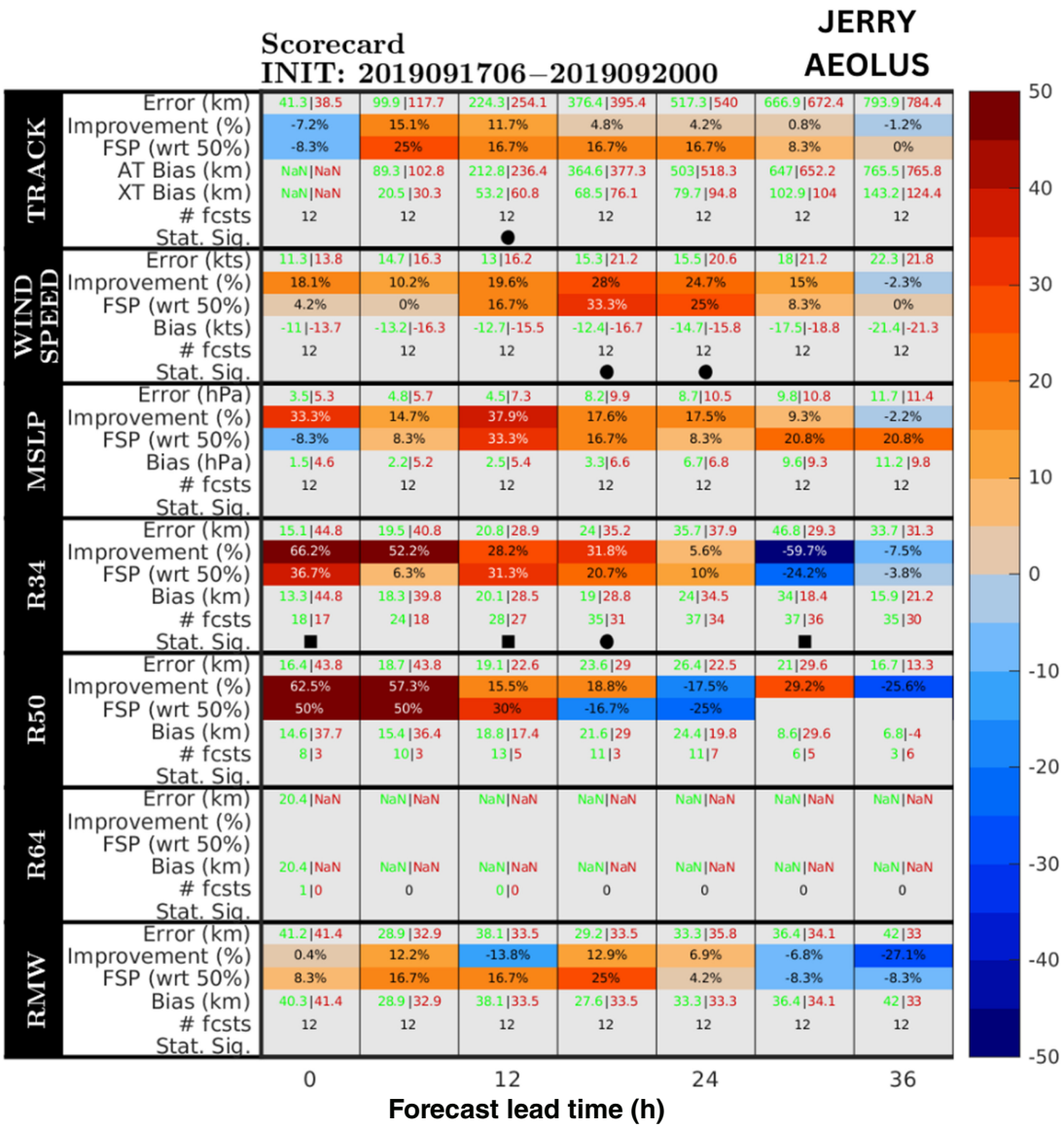

FIGURE 9 Scorecard for AL category two hurricane Jerry19 for the AEOLUS experiment, up to the 36th forecast lead time hour. Statistical significance is displayed as 95% (squares) and 90% (circles) confidence intervals with respect to the CONTROL experiment. Warm colors indicate improvements, while cool colors indicate degradations [Colour figure can be viewed at wileyonlinelibrary.com]

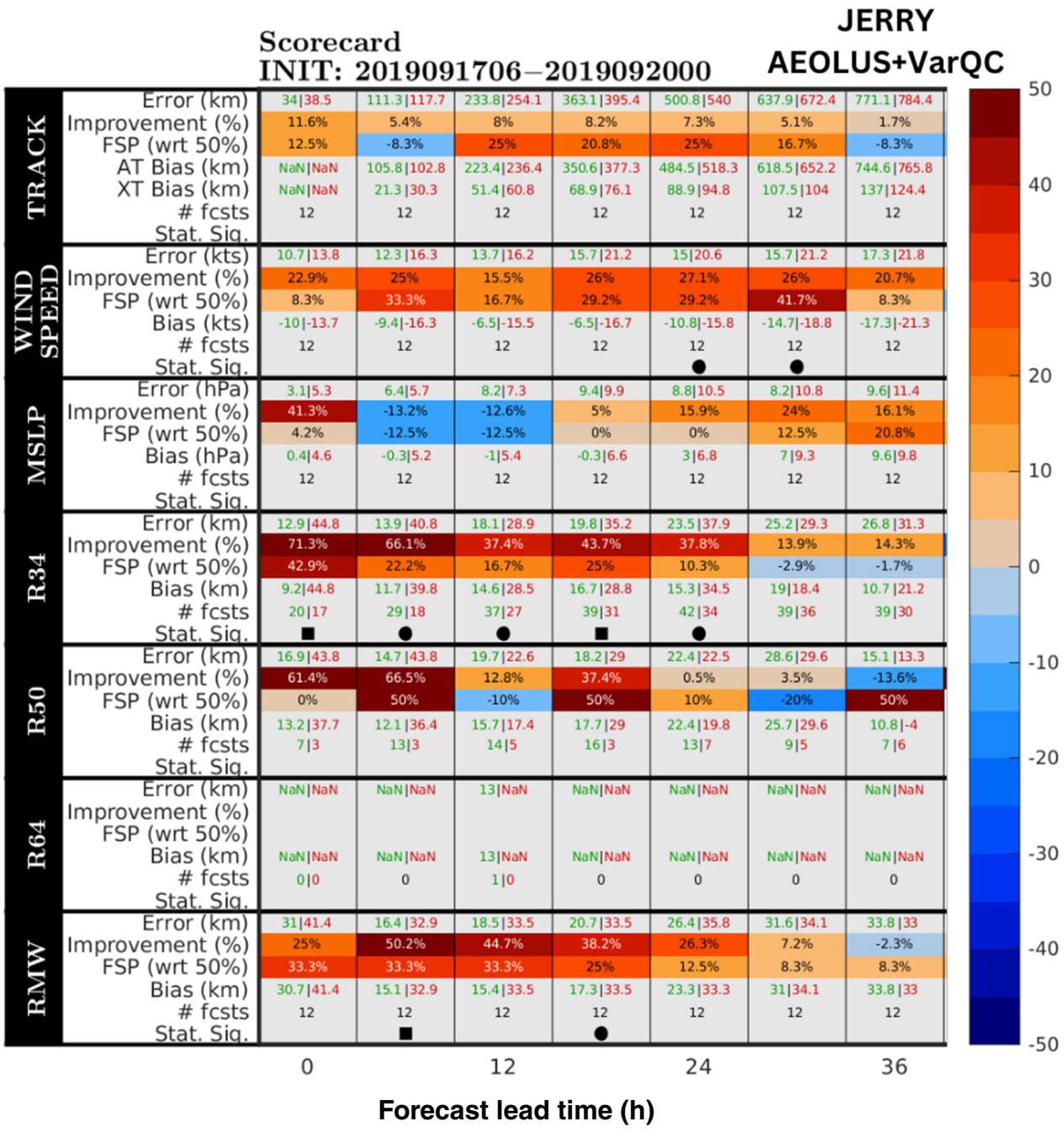

FIGURE 10 Scorecard for AL category two hurricane *Jerry19* for the AEOLUS + VarQC experiment, up to the 36th forecast lead time hour. Statistical significance is displayed as 95% (squares) and 90% (circles) confidence intervals with respect to the CONTROL experiment. Warm colors indicate improvements, while cool colors indicate degradations [Colour figure can be viewed at wileyonlinelibrary.com]

also indicated differences in the vertical location of the assimilated observations and that variations from cycle to cycle occurred. The lifetime of each storm was also a contributing factor, with longer storm lifetimes having an increased likelihood of collocation with Aeolus overpasses.

As mentioned in Section 2, VarQC aims to improve the calculation of an optimal analysis by assigning adaptive observation weights. To evaluate if the use of VarQC could improve the initialization of TCs and short-range forecasts, an initial assessment of two category 1–2 hurricanes on the AL and EP basins was conducted. We followed a verification approach similar to that in the Marinescu *et al.* (2022) study and evaluated the impact of assimilating Aeolus data on GFS_v16.0 forecasts of relevant tropical cyclone metrics using scorecards. Seven metrics were used to evaluate storm track, intensity, and TC size. Scorecard plots include the following error metrics: storm TRACK (km); surface WIND SPEED (kts);

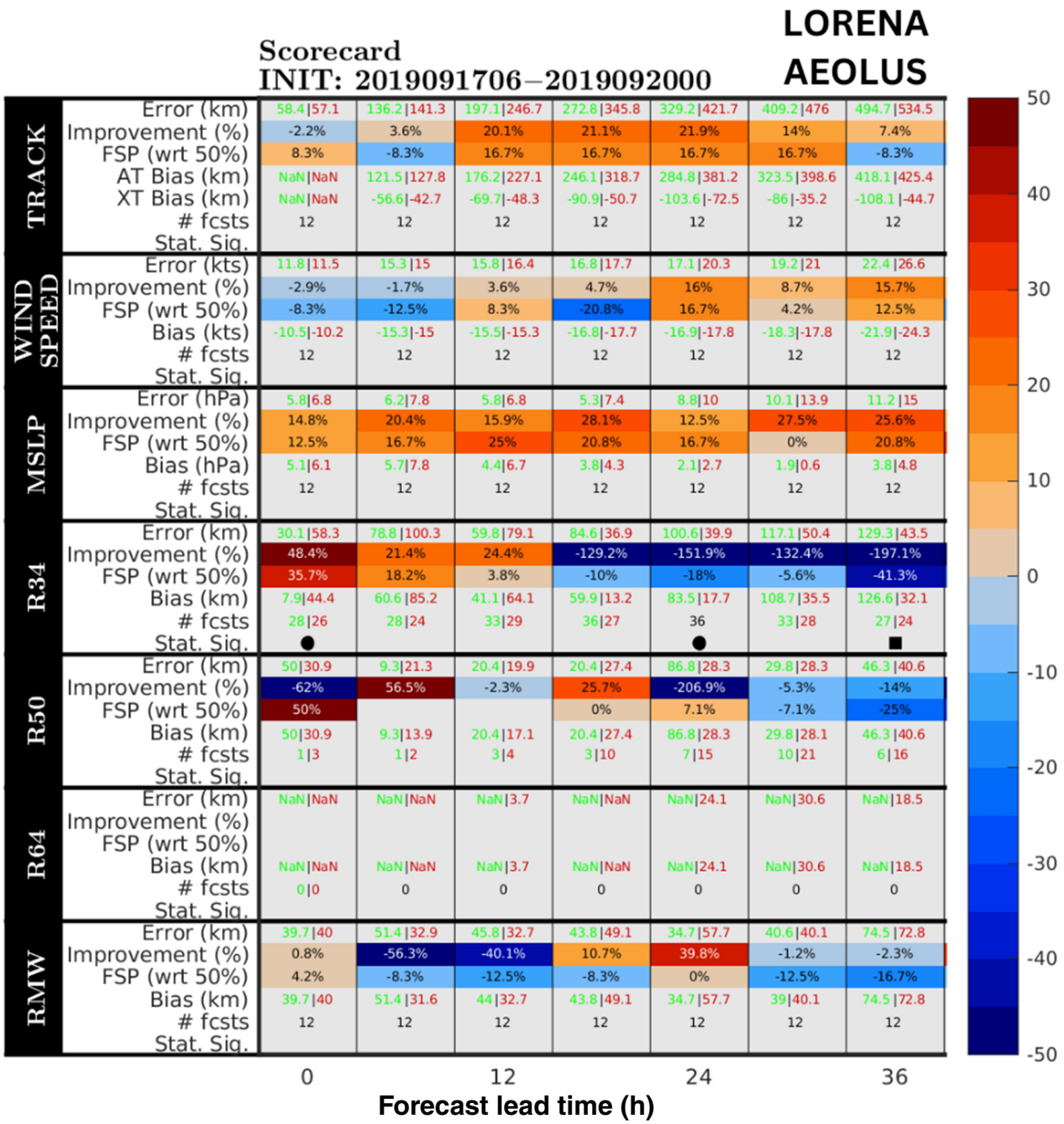

FIGURE 11 Scorecard for East Pacific (EP) category one hurricane *Lorena19* for the AEOLUS experiment, up to the 36th forecast lead time hour. Statistical significance is displayed as 95% (squares) and 90% (circles) confidence intervals with respect to the CONTROL experiment. Warm colors indicate improvements, while cool colors indicate degradations [Colour figure can be viewed at wileyonlinelibrary.com]

minimum sea level pressure (MSLP in hPa); the radii of tropical-storm-force winds (R34, km), storm-force (R50, km), and hurricane-force (R64, km) winds. These metrics were compared to the Hurricane Database (HURDAT-2) best estimates from the National Hurricane Center (Landsea and Franklin, 2013).

Comparing the scorecards for the AEOLUS (Figure 9) and AEOLUS + VarQC (Figure 10) experiments for hurricane *Jerry* in the AL basin indicate an improved initialization in the AEOLUS+ VarQC experiment. TRACK, WIND SPEED, MSLP, R34, and the radius of maximum winds (RMW) error metrics show improvements at the 0-hr Forecast Lead Time (FLT). Since this is a global model, these positive changes were also likely deriving from the assimilation of additional Aeolus profiles on the peripheral storm environment through the VarQC.

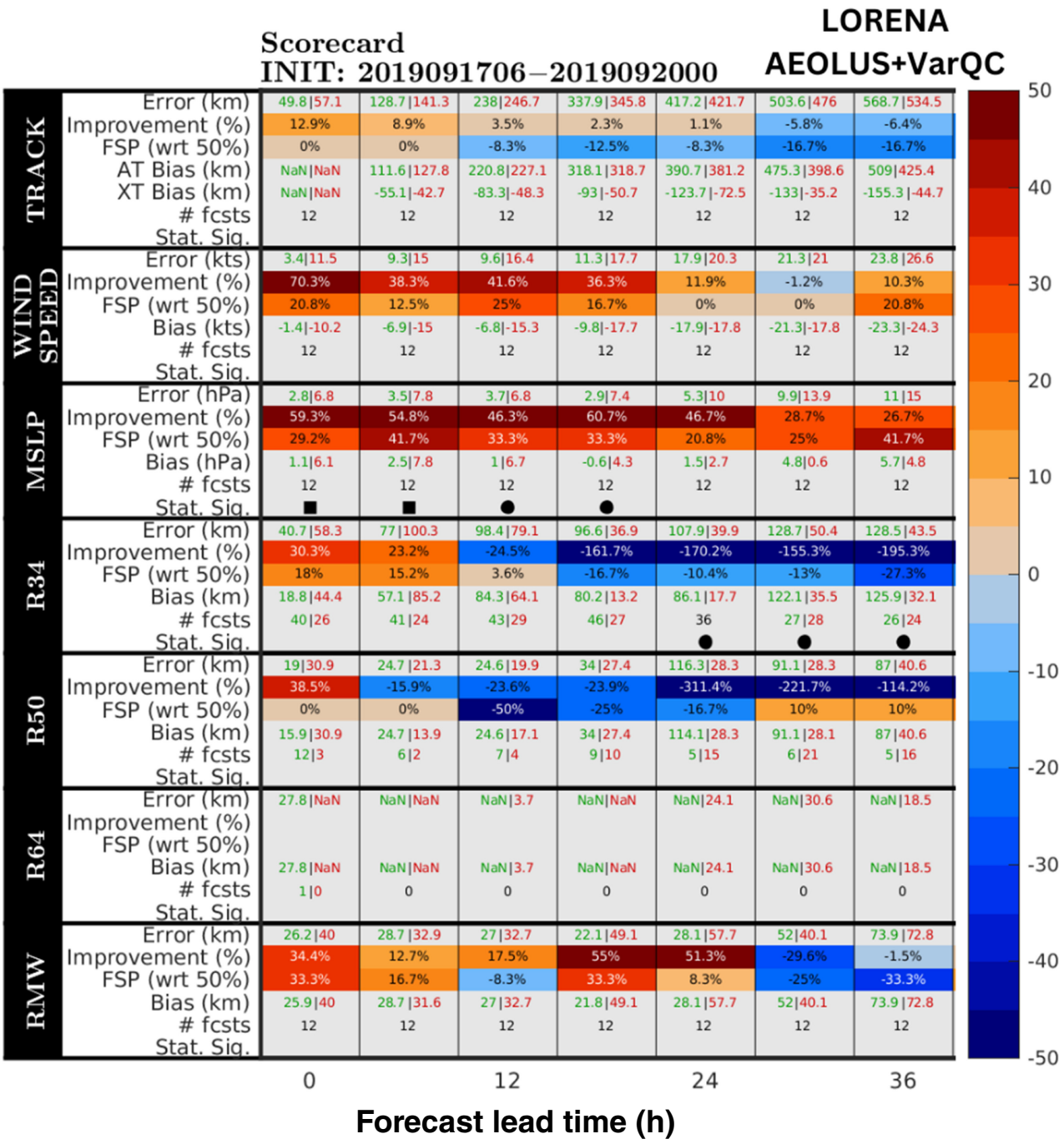

FIGURE 12 Scorecard for East Pacific (EP) category one hurricane *Lorena19* for the AEOLUS+VarQC experiment, up to the 36th forecast lead time Statistical significance is displayed as 95% (squares) and 90% (circles) confidence intervals with respect to the CONTROL experiment. Warm colors indicate improvements, while cool colors indicate degradations [Colour figure can be viewed at wileyonlinelibrary.com]

A degradation or decreased improvement percentage was seen at the six-hour FLT, followed by improvements up to the 30th-hour FLT for the AEOLUS +VarQC experiment on the same metrics. The radius of tropical-storm-force winds (R34) and RMW show statistically significant improvements, as indicated by the filled squares and circles.

A similar comparison between the scorecards of the AEOLUS (Figure 11) and AEOLUS + VarQC (Figure 12) was made for EP category 1 hurricane *Lorena*. Figure 12 shows a better initialization in the AEOLUS + VarQC experiment for most metrics. The TRACK forecast was also degraded, but MSLP indicated statistically significant improvements. This initial assessment indicates a benefit

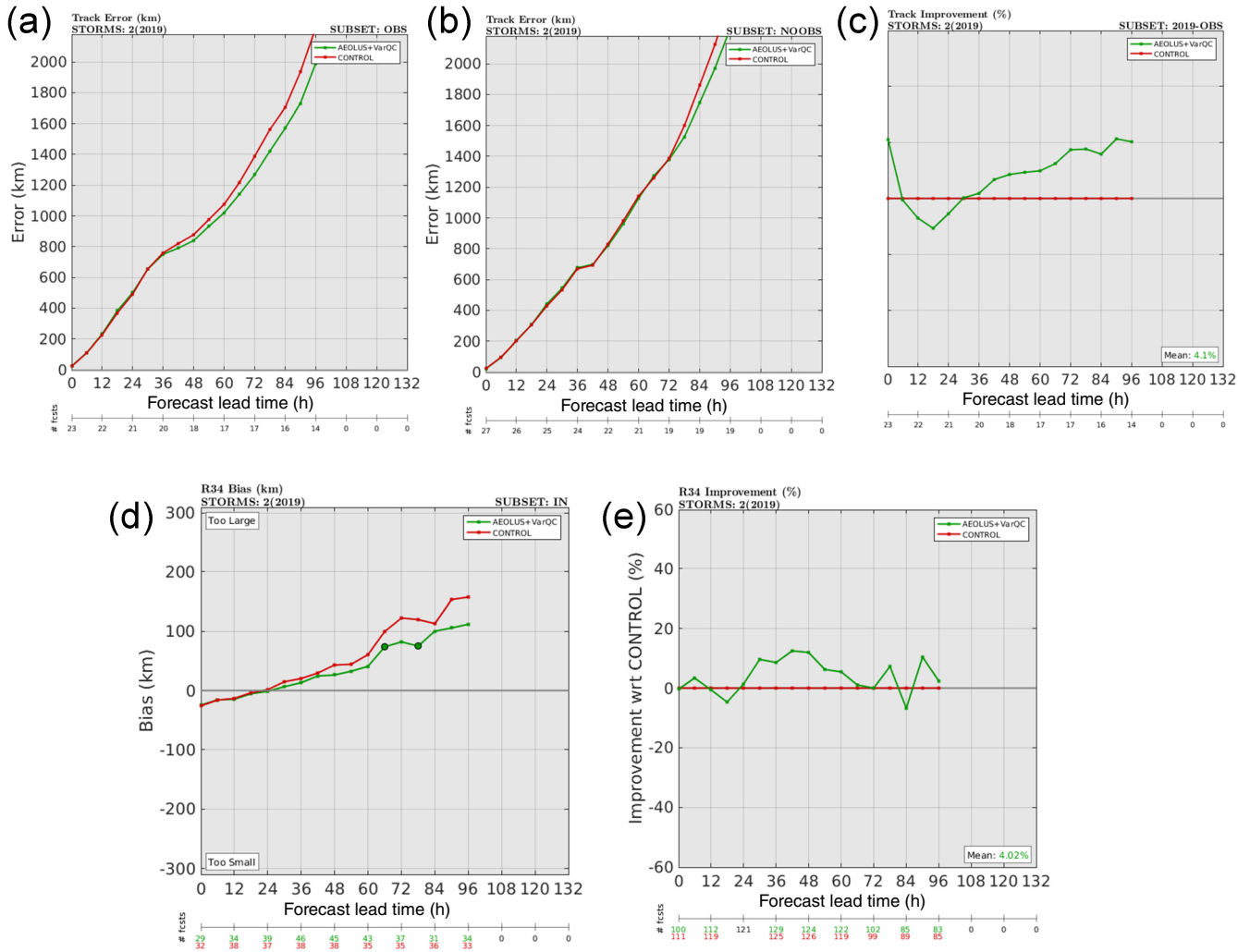

FIGURE 13 (a) Composite track error for 2019 *Dorian* and *Erin*, for the CONTROL (red) and AEOLUS + VarQC (green) for the (a) OBS subset; (b) NOOBS subset; (c) track improvement percentage; (d) radius of 34 km winds for the rapid intensification stage; (e) percentage improvement in the radius of 34 km error [Colour figure can be viewed at wileyonlinelibrary.com]

on the initialization of TCs by assimilating AEOLUS with VarQC. Nonetheless, evaluating a larger sample of TC cases would provide a more robust forecast impact assessment.

4.5 | CONTROL vs. AEOLUS + VarQC composite tropical cyclone verification for the 2019 Atlantic-basin hurricane *Dorian* and tropical storm *Erin*

Since the ultimate goal of the NCEP-VQC is to allow more observations to be assimilated, let us discuss the general impact of Aeolus observations on tropical cyclone forecasting. This Section shows a comparison of a CONTROL experiment to an AEOLUS + VarQC experiment. The CONTROL experiment included the suite of observations operationally assimilated by the NOAA/NCEP. It had the same settings as the AEOLUS + VarQC expNCEPeriment, except we did not assimilate any Aeolus profiles, and the NCEP-VQC algorithm was turned off. The impact of Aeolus on tropical cyclone metrics was evaluated for a major hurricane (category 5 hurricane AL *Dorian*, 2019) and a tropical storm (AL *Erin*, 2019). In Figure 13, composite plots of track error in kilometers and percentage improvement indicate that the AEOLUS + VarQC experiment outperforms the CONTROL when Aeolus observation are present (OBS subset) in the vicinity of the storms, with a 4.1% improvement on (c) track in the OBS subset of the AEOLUS + VarQC (green) experiment with respect to CONTROL (red) after the 36-hr FLT. The improvement was significant for the cycles in which the storms were undergoing rapid intensification, particularly in (d) the radius of 34-knot winds with a mean improvement of

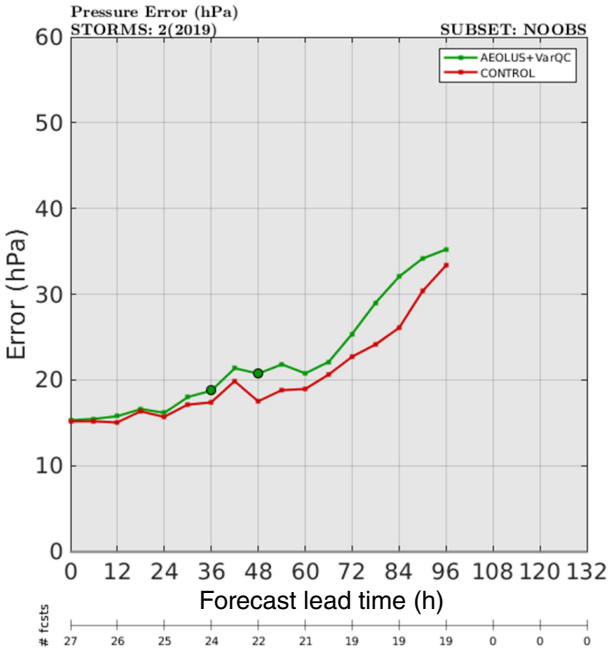

FIGURE 14 Pressure error in hPa for the subset where no Aeolus wind profiles (NOOBS) were present in the vicinity of the storm [Colour figure can be viewed at wileyonlinelibrary.com]

4.02% (e). This highlights the importance of having Aeolus observations present when a TC is undergoing rapid intensification.

Composite graphics of pressure error in hPa for storms *Erin* and *Dorian* indicate statistically significant degradation (Figure 14) for the subset of cycles without the assimilation of Aeolus profiles (NOOBS) after the 24 hr FLT. For the case of *Dorian*, it was possible to pinpoint the location of the assimilated Aeolus observations with respect to the TC path and storm center. Figure 15a shows that Aeolus orbits intersected the TC track when the storm underwent rapid intensification but significantly less during the weakening stages. Figure 15b shows that the highest number of assimilated observations occurs at the 1,500 m radius. After inspecting the error in the location of 34-knot tropical-storm-force winds for *Dorian* (Figure 16a), a 12.33% improvement was estimated (Figure 16b) during the rapid intensification subset after the 72 hr FLT and a statistically significant instance of error reduction during the tropical storm stage subset (Figure 16c).

5 | CONCLUSIONS

Motivated by the positive benefits from the assimilation of Aeolus HLOS wind profiles in weather analyses and forecasts, we implemented, tested, and quantified here the use of the NCEP-VQC algorithm as additional observational quality control for Aeolus observations. The advantage of using VarQC is that, when it is applied during the minimization step of the variational analysis procedure, the information regarding the a-priori estimates of relevant sources of error and the analysis state is considered and used synergistically. Our results show that this added QC is beneficial in analyzing and forecasting TCs, where observations deviate significantly from the model background.

It is important to note that the use of VarQC does not replace the ESA-recommended static quality controls for the Aeolus Mie-cloudy and Rayleigh-clear wind profiles but rather allows the relaxation of the QC limits and the handling of observations outliers leading to an increase in the number of retained observations.

The assimilation of Aeolus's observations was improved, assuming their errors follow a family of logistic distributions. Furthermore, assimilating Aeolus with additional VarQC proved a consistent retention of more wind profiles during the six tropical cyclone cases analyzed in this study. Improvements in the initialization and short-range forecasts of TCs in NOAA's global forecast model were observed during eight tropical cyclone case studies of the 2019 hurricane season. However, before NOAA begins to assimilate Aeolus wind profiles operationally –most likely to happen if there is an Aeolus follow-on mission – and apply NCEP-VQC to the assimilation process, it would be beneficial to conduct a forecast impact assessment of up to two hurricane seasons to determine if the initial positive results seen in this study can be reproduced with a high degree of statistical significance. This type of careful impact assessment and optimized QC would be extremely beneficial in preparation for the anticipated Aeolus-2 follow-on mission, expected to launch in or after 2031.

To the best of our knowledge, the present study is the first attempt to apply VarQC to satellite wind observations. For this reason, we were cautious when we loosened the OE limits. Therefore, additional experiments in which the OE limits would be further relaxed are recommended, particularly when assimilating low-accuracy data, such as Aeolus Raleigh-clear winds alongside operationally used AMVs. Nonetheless, this study shows the strength and benefits of performing VarQC when some observations deviate significantly from the model background; without adaptive weight assignment, accurate and/or beneficial observations can be arbitrarily discarded.

AUTHOR CONTRIBUTIONS

Karina Apodaca: Conceptualization; formal analysis; investigation; methodology; software; validation; writing – original draft. **Lidia Cucurull:** Funding acquisition; project administration; supervision; writing – review and editing. **Iliana Genkova:** Investigation; software;

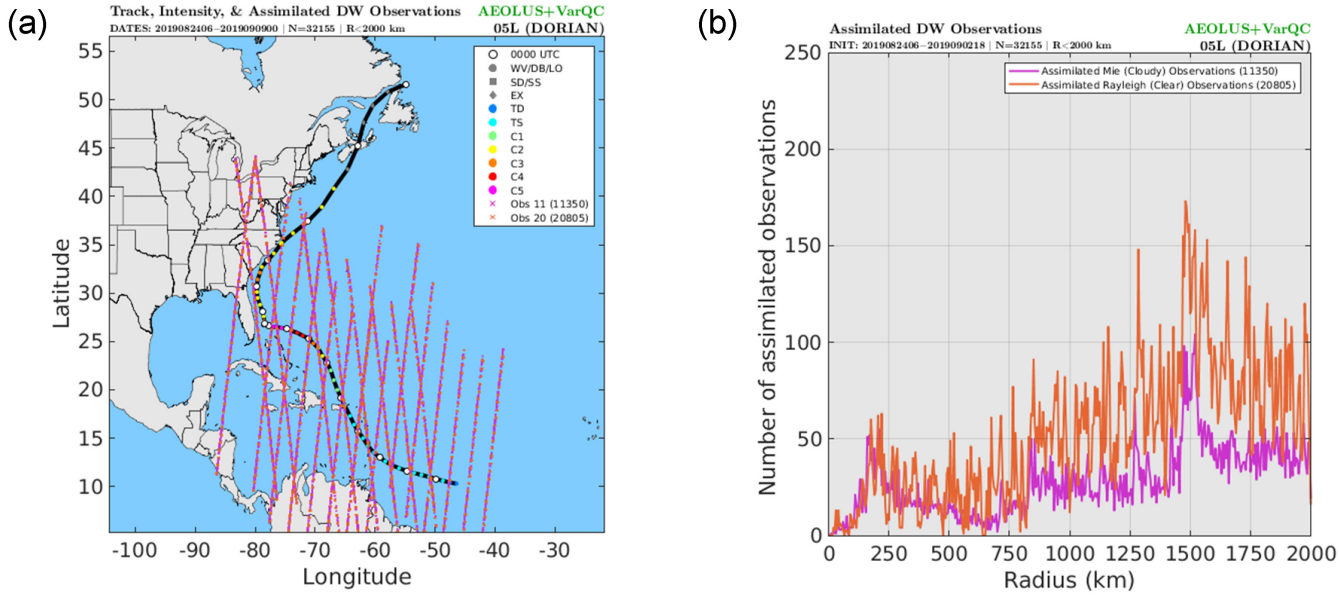

FIGURE 15 (a) Location of assimilated Aeolus observations with respect to the TC path and (b) radius from the TC center [Colour figure can be viewed at wileyonlinelibrary.com]

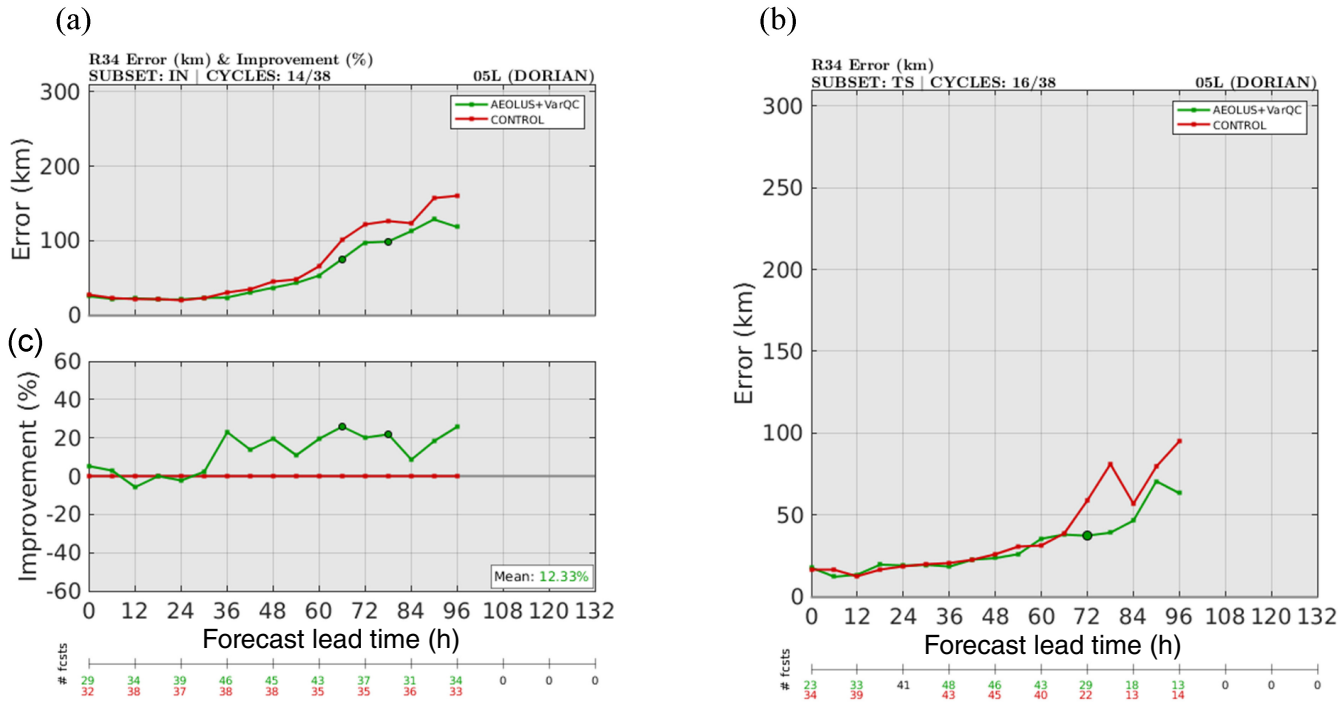

FIGURE 16 (a) Error in the location of the radius of 34-knot winds for the intensifying stage and (b) percentage improvement; (c) radius of 34-knot winds location error in km during the tropical cyclone phase [Colour figure can be viewed at wileyonlinelibrary.com]

validation; writing – review and editing. **Jim James Purser:** Software; writing – review and editing. **Xiujuan Su:** Software.

ACKNOWLEDGEMENTS

This research was funded by the NOAA/NESDIS-/OPPA/Technology Maturation Program under the NOAA-CIMAS Grant No. GR003756/665653. The authors are grateful to the following individuals: Sarah Ditchek (CIMAS), Keren Rosado (NWS), Paulo Paz (CIMAS), Andrew Kren (NWS), and Claude Gibert (Spire Global, Inc.) for their assistance with various plotting resources. Peter Marinescu from (CSU/CIRA) for his assistance with data curation. Lisa Bucci (NOAA/AOML) for her scientific

guidance on selecting tropical cyclone case studies. The entire Aeolus TMP-1 team, with special thanks to Mike Hardesty (CIRES), Kayo Ide (UMD), Hui Liu (ESSIC), and Kevin Garrett (NOAA/STAR) for the fruitful collaboration and insightful comments. Will McCarty (NASA) for providing the initial subroutines for processing the Aeolus data in GSI. NOAA/OAR/AOML for providing the NOAA HPC accounts and computing resources to carry out this research. Daryl T. Kleist for reviewing this manuscript and providing useful edits and valuable comments. Professor Nedjeljka Žagar for stepping in as an additional reviewer, providing very insightful comments, which greatly improved the quality and presentation of this manuscript. Anonymous reviewers who took the time to make very thorough reviews and for providing comments that greatly enhanced the quality of this manuscript.

ORCID

Karina Apodaca https://orcid.org/0000-0001-5502-5289

REFERENCES

Andersson, E. and Järvinen, H. (1999) Variational quality control. *Quarterly Journal of the Royal Meteorological Society*, 125, 697–722.

Apodaca, K., Cucurull, L., Genkova, I., Purser, R.J., Su, X., Bucci, L., Marinescu, P.J., Liu, H. and Garrett, K. (2020) Assessment of data assimilation techniques for improved use of Aeolus wind profiles in NOAA's NWP systems with a focus on TC predictability. In: *[Proceedings/Conference presentation]. 2nd ESA Aeolus Cal/Val and Science workshop, Virtual, 2—6 November 2020*.

Applications: Aeolus Satellite. (2022) ESA. https://www.esa.int/Applications/Observing_the_Earth/FutureEO/Aeolus/Aeolus_satellite.

Derber, J.C., Parrish, D.F. and Lord, S.J. (1991) The new global operational analysis system at the National Meteorological Center. *Weather and Forecasting*, 6, 538–547. https://doi.org/10.1175/2009WAF2222201.1.

Farrar, M. (2021) Upgrade NCEP Global Forecast Systems (GFS) to v16: Effective March 22, 2021. Service Change Notice 21–20 Updated. https://www.weather.gov/media/notification/pdf2/scn21-20_gfsv16.0_aac.pdf.

George, G., Halloran, G., Kumar, S., Rani, S.I., Bushair, M.T., Jangid, B.P., George, J.P. and Maycock, A. (2021) Impact of Aeolus horizontal line of sight wind observations in a global NWP system. *Atmospheric Research*, 261, 105742. https://doi.org/10.1016/j.atmosres.2021.105742.

Ingleby, N.B. and Lorenc, A.C. (1993) Bayesian quality control using multivariate normal distributions. *Quarterly Journal of the Royal Meteorological Society*, 119, 1195–1225.

Kleist, D.T. and Ide, K. (2015) An OSSE-based evaluation of hybrid variational-ensemble data assimilation for the NCEP GFS. Part I: System description and 3D-hybrid results. *Monthly Weather Review*, 143, 433–451.

Kleist, D.T., Parrish, D.F., Derber, J.C., Treadon, R., Wu, W.-S. and Lord, S. (2009) Introduction of the GSI into the NCEP global data assimilation system. *Weather and Forecasting*, 24, 1691–1705. https://doi.org/10.1175/2009WAF2222201.1.

Landsea, C.W. and Franklin, J.L. (2013) Atlantic hurricane database uncertainty and presentation of a new database format. *Monthly Weather Review*, 141, 3576–3592. https://doi.org/10.1175/MWR-D-12-00254.1.

Liu, H., Garrett, K., Ide, K., Hoffman, R. and Lukens, K. (2022) A statistically optimal analysis of systematic differences between Aeolus HLOS winds and NOAA's global forecast system. *Atmospheric Measurement Techniques*, 15, 3925–3940, 2022. https://doi.org/10.5194/amt-15-3925-2022.

Lorenc, A.C. and Hammon, O. (1988) Objective quality control of observations using Bayesian methods – theory, and practical implementation. *Quarterly Journal of the Royal Meteorological Society*, 114, 515–543.

Marinescu, P.J., Cucurull, L., Apodaca, K., Bucci, L. and Genkova, I. (2022) The characterization and impact of Aeolus wind profile observations in NOAA's regional tropical cyclone model (HWRF). *Quarterly Journal of the Royal Meteorological Society*, 148, 3491–3508. https://doi.org/10.1002/qj.4370.

Martin, A., Weissmann, M., Reitebuch, O., Rennie, M., Geiß, A. and Cress, A. (2021) Validation of Aeolus winds using radiosonde observations and numerical weather prediction model equivalents. *Atmospheric Measurement Techniques*, 14, 2167–2183. https://doi.org/10.5194/amt-14-2167-2021.

Purser, R.J. (2018) Convenient parameterization of super-logistic probability models of effective observation error. *NOAA/NCEP Office Note* 495, 8. https://doi.org/10.25923/kvmz-vf34.

Rennie, M. and Isaksen, L. (2020) *The NWP Impact of Aeolus Level-2B Winds at ECMWF*. Reading, UK. Available from: *ECMWF* Technical memorandum 864. ECMWF https://www.ecmwf.int/node/19538.

Rennie, M., Isaksen, L., Weiler, F., De Kloe, J., Kanitz, T. and Reitebuch, O. (2021) The impact of Aeolus wind retrievals in ECMWF global weather forecasts. *Quarterly Journal of the Royal Meteorological Society*, 147, 3555–3586. https://doi.org/10.1002/qj.4142.

Savli, M., de Kloe, J., Marseille, G.J., Rennie, M., Zagar, N. and Wedi, N. (2019) The prospects for increasing the horizontal resolution of the Aeolus horizontal line-of-sight wind profiles. *Quarterly Journal of the Royal Meteorological Society*, 145, 3499–3515. https://doi.org/10.1002/qj.3634.

Straume, A.G., Rennie, M., Isaksen, L., de Kloe, J., Marseille, G.-J., Stoffelen, A., Flament, T., Stieglitz, H., Dabas, A., Huber, D., Reitebuch, O., Lemmerz, C., Lux, O., Marksteiner, U., Weiler, F., Witschas, B., Meringer, M., Schmidt, K., Nikolaus, I., Geiss, A., Flamant, P., Kanitz, T., Wernham, D., Bismarck, J., von Bley, S., Fehr, T., Floberghagen, R. and Parinello, T. (2020) ESA's space-based doppler wind lidar Mission Aeolus – first wind and aerosol product assessment results. *EPJ Web of Conferences*, 237, 01007. https://doi.org/10.1051/epjconf/202023701007.

Tavolato, C.L. and Isaksen, L. (2014) On the use of a Huber norm for observation quality control in the ECMWF 4D-var. *Quarterly Journal of the Royal Meteorological Society*, 141, 1514–1527.

The Graphics for OSEs and OSSEs on TCs (n.d.). (GROOT) verification package developed by Dr. Sarah Ditchek and funded by the Quantitative Observing System Assessment Program (QOSAP) and the FY18 Hurricane Supplemental (NOAA Award ID #NA19OAR0220188) was used to generate graphics for this publication.

Weiler, F., Rennie, M., Kanitz, T., Isaksen, L., Checa, E., de Kloe, J., Okunde, N. and Reitebuch, O. (2021) Correction of wind bias for the lidar on board Aeolus using telescope temperatures. *Atmospheric Measurement Techniques*, 14, 7167–7185. https://doi.org/10.5194/amt-14-7167-2021.

Zuo, H., Hasager, C.B., Karagali, I., Stoffelen, A., Marseille, G.-J. and de Kloe, J. (2022) Evaluation of Aeolus L2B wind product with wind profiling radar measurements and numerical weather prediction model equivalents over Australia. *Atmospheric Measurement Techniques*, 15, 4107–4124. https://doi.org/10.5194/amt-15-4107-2022 2022.

How to cite this article: Apodaca, K., Cucurull, L., Genkova, I., Purser, R.J. & Su, X. (2023) Assessing the benefit of variational quality control for assimilating Aeolus Mie and Rayleigh wind profiles in NOAA's global forecast system during tropical cyclones. *Quarterly Journal of the Royal Meteorological Society*, 149(756), 2761–2783. Available from: https://doi.org/10.1002/qj.4530